Semi-Analytical Modelling of Tuned Liquid Damper (TLD) with Emphasis on Damping of Liquid Sloshing

液体動揺減衰に注目した
同調液体ダンパー（ＴＬＤ）のモデル化

by
SUN Limin
孫　利民

Thesis submitted to the University of Tokyo
in partial fulfillment of requirements
for the Doctor of Engineering degree

September, 1991

ACKNOWLEDGEMENTS

I am especially grateful to my thesis advisor, Professor Yozo Fujino, who suggested the topic and offered the most valuable guidance and encouragement throughout this study. I am also greatly indebted to Prof. Manabu Ito, Asso. Prof. Benito M. Pacheco and Assoc. Prof. Takashi Nomura for their advices. I would like to express my gratitude to Assoc. Prof. Masahiko Isobe of University of Tokyo for his informative discussion on hydrodynamics and wave theories.

Professor Nobuyuki Tamai, Assoc. Prof. Jun Kanda, Assoc. Prof. Masahiko Isobe and Asso. Prof. Fumio Yamazaki are the members of my thesis committee. I wish to thank all of them for giving me comments and suggestions.

I am also grateful to Dr. P. Chaiseri, Mr. K. Koga, Mr. K. Nozawa, Mr. S. Kaneko and other students and colleagues in Bridge and Structure Lab. of Civil Engineering Department for their comments and assistances.

In addition, I would also like to thank Dr. K. Fujii and Mr. T. Ohtsuki, Shimizu Corporation, for allowing use of the shaking table facility and giving suggestions during the experiment.

I thank the Japan Ministry of Education, Science and Culture for providing me with a scholarship through three years of my graduate studies. This study is partially supported by the Grant-in-Aid for Developmental Scientific Research from the Japan Ministry of Education, Science and Culture, and by the Cooperative Research with Shimizu Corporation.

My fiancee, Ye Zheng, encouraged me and provided me with strong support through her love and patience.

ABSTRACT

The properties of Tuned Liquid Damper are investigated theoretically and experimentally in this study. Tuned Liquid Damper (TLD) is a kind of passive mechanical damper which relies on the sloshing of shallow liquid in a rigid tank for suppressing structural vibrations. Recent growing interest in liquid dampers is attributable to several potential advantages, including: low costs; easy to install in existing structures; applicable for temporary use; non-restriction to uni-directional excitation; and effective even for small-amplitude vibrations.

The author has previously proposed a nonlinear model for a rectangular TLD under horizontal motion on the basis of the shallow water wave theory. In this study, the model is improved with emphasis on the damping of liquid sloshing, which is a significant parameter affecting the effectiveness of TLD. The model is expanded to accommodate liquid sloshing in a rectangular TLD tank under pitching motion. Breaking waves which occur in shallow liquid sloshing are taken into account in the model.

Two types of experiments were carried out in order to study the properties of the liquid sloshing in TLD as well as to assess the validity of the model proposed. One is a shaking table experiment, in which the TLD is sinusoidally excited by horizontal motion or pitching motion. The properties of TLD, such as nonlinearities and damping, are investigated on the basis of the experimental results. Another type of experiment, namely TLD-structure interaction experiment is, conducted in order to demonstrate the effectiveness of TLD for suppressing structural vibration. The TLD-structure system used in the experiment consists of a SDOF structure and a TLD attached. The effects of parameters of TLD, such as damping of liquid sloshing, on its effectiveness are also discussed.

The shaking table experiments show that the liquid sloshing is vary nonlinear and reveals a hardening-spring property when the liquid is shallow. The higher harmonics whose natural frequencies are approximately odd number times of the fundamental one, contribute some effects near the primary resonance and made the liquid sloshing properties more complicated. The proposed model is assessed by the experimental results; it is shown that the model can predict surface elevation, base shear force, as well as energy dissipation per cycle of liquid sloshing with a good accuracy. The TLD-structure interaction experiment shows that the structural response is reduced significantly by attaching TLD to the structure, indicating that TLD is very effective. The simulations of TLD-structure

interaction based on the proposed model agree well with the experimental results.

The SOLA-VOF code is employed to simulate liquid sloshing in the present of breaking waves. It is, however, found that the code is not valid for an engineering application to predict the liquid sloshing with breaking waves. The proposed model is therefore modified for accounting for breaking waves. Two coefficients introduced into the basic equations and these are determined from a systematic shaking table experiment. The empirical formulas are expressed as a function of the dimensionless amplitude of excitation. With this modified TLD model, it is show that the response of structure attached with TLD can be simulated with a satisfactory accuracy even when the breaking waves present in TLD.

The basic parameters affecting the properties of TLD are discussed; these parameters in turn are affected by several physical quantities such as TLD tank size, liquid depth ratio, and liquid viscosity. The discussions on the relations between TLD basic parameters and those physical quantities may be helpful for TLD design. The mechanism of TLD is briefly explained based on the understanding of the mechanism of Tuned Mass Damper (TMD). It is also shown that the effectiveness of TLD could become comparable with that of TMD if the damping of liquid sloshing is controlled to a suitable level. The experimental investigations are also carried out to increase the damping of liquid sloshing to make TLD more effective. The experimental results show that the effectiveness of TLD can be improved by employing several means e.g., using shallow liquid; using high-viscous liquid; and adding floating materials on liquid surface.

The multiple TLD's (MTLD), which consists of a number of TLD's with natural frequencies distributed over certain range around the natural frequency of the structure, is also investigated by simulation of the MTLD-structure interaction. It is found that MTLD is very efficient to suppress the structural vibration even each TLD has small damping. In practice, TLD is designed to consist of a number of TLD's with the same size to meet required liquid mass. Multiple TLD's are easy to be designed by varying the liquid depth in each TLD to have distributed natural frequencies. It is also found that MTLD is insensitive to the tuning condition. Since the effectiveness of MTLD is very good when the damping of liquid sloshing is low, the plain water can be used as the liquid of TLD. MTLD is a valuable concept for TLD design application.

TABLE OF CONTENTS

CHAPTER 1 INTRODUCTION

1.1 TUNED LIQUID DAMPER

Light, flexible, and weakly-damped civil engineering structures, such as tall buildings, towers and long span bridges, have been increasing in number. Vibrations of such structures due to wind, earthquake and other dynamic disturbances can cause problems from serviceability or safety viewpoint. Various techniques, such as base isolation devices, passive or even active control devices are proposed to damp the structural vibrations. The installation of a passive device including mechanical dampers is also one way and becoming common to suppress undesirable vibrations [Fujino 1990].

Figure 1.1 Tuned Liquid Damper (TLD) installed on a building and Tower (Size of TLD is not in Scale).

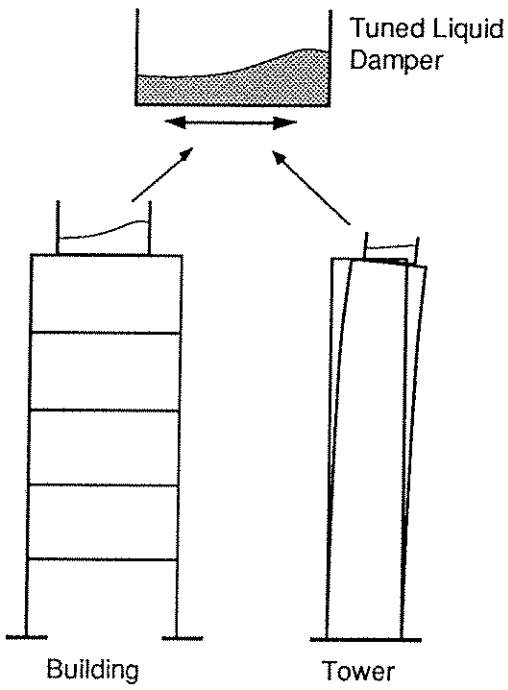

This thesis is concerned with a new type of passive mechanical damper, named *Tuned Liquid Damper* (TLD) (Fig. 1.1), which relies on the sloshing of shallow liquid inside a rigid tank, for changing the dynamic characteristics of a structure and dissipating its vibration energy [Fujino et al. 1988]. Dampers using liquid sloshing have been in use in space satellites and marine vessels [Bhuta and Koval 1966, Sayar and Baumgerten 1982, Watanabe 1969]. Recent growing interest in liquid dampers for application to ground structures [e.g., Modi and Welt 1987, Fujii et al. 1988, Sakai et al. 1990, and Chaiseri 1989] is attributable to several potential advantages, including: low cost; easy installation especially in existing structures which often have severe space constraints; adaptability to temporary use; almost zero trigger level; non-restriction to uni-directional excitation; and few maintenance requirements.

Liquid sloshing in a closed basin have been studied by many researches [e. g., Chester 1968, Miles 1976] for applying to the harbor problems in the field of coastal engineering. Lepellelier [1980] has reviewed the literatures pertaining the liquid sloshing problem. The liquid sloshing problems were also investigated in space field [Abramson 1966]; the liquid sloshing in spacecraft and launch vehicles fuel tanks have been extensively studied. Researches on the sloshing problems in storage tanks under earthquake have been also done [Sogabe, Shibata 1974]. Compared with the problems mentioned above, the liquid sloshing in TLD has some special aspects; these are:

(i) The liquid in TLD is shallow in order to attain higher damping and a low natural frequency to tune to a civil engineering structure. The shallow liquid leads that the liquid sloshing has very strong nonlinearities so that a linear theory is not satisfactory for treating the problem.

(ii) The damping of liquid sloshing is a significant parameter affecting the effectiveness of TLD and should be carefully treated.

(iii) Breaking waves may present in liquid sloshing in TLD under large amplitude base motion. A model which can account for breaking waves has to be developed.

Modelling of TLD has been studied by several researchers [e.g., Modi 1987, Sato 1987, Noji 1988 and Miyata 1989]. Linear [Sato 1987] and nonlinear TMD Analogy models [Chaiseri 1990] were proposed. However, because of the strong

nonlinearities of shallow liquid sloshing in TLD, these models could not give satisfactory results. Numerical simulations by BEM [Ohyama 1989] can accurately describe nonlinear liquid sloshing, however, computational time is imperative.

Modi and Welt [1987, 1989] carried out an experimental and analytical study on the nutation damper (annular tank) which is conceptually the same as TLD, and they investigated the energy dissipation mechanism of the nutation damper using a nonlinear potential flow model in conjunction with the boundary layer correction. Experimental studies on rectangular TLD are also available (e.g.' , Miyata et al. 1988), but an adequate mathematical model for rectangular TLD is insufficient.

1.2 SCOPE OF STUDY

The objectives of this study are to propose models of rectangular TLD and to investigate the TLD properties experimentally and theoretically. Moreover, the means increasing effectiveness of TLD are studied.

A nonlinear model of liquid sloshing inside a rectangular TLD, which was recently developed by the author [Sun. 1988] based on the shallow water wave theory , is refined with emphasis on damping of liquid sloshing in this thesis. The model is furthermore extended to deal with the liquid sloshing in TLD subjected to pitching motion. It will be shown that the models are in good agreement with the experiment in the region of relatively small vibration amplitude where breaking waves in TLD do not occur. To account for breaking waves, the proposed model is modified by introducing two empirically identified coefficients.

Based on the models of liquid sloshing , the interaction of TLD and structure is next studied , and the performance of a rectangular TLD attached to a structure which is subjected to an external harmonic force is discussed. Experiment is also carried out to confirm the validity of the TLD models as well as the effectiveness of TLD. The studies on the damping of liquid sloshing are one of the main parts.

Chapter 2 presents the theoretical parts of the study. The linear theory of liquid sloshing in a rectangular tank is explained and the properties of liquid sloshing are discussed. A nonlinear model for TLD subjected to horizontal motion is proposed on the basis of the shallow liquid theory. The damping of

liquid sloshing is included in the model. Moreover, the model is extended to simulate the liquid sloshing in TLD subjected to pitching motion. The principle of SOLA-VOF code which is employed to simulate liquid sloshing with breaking waves is explained.

Chapter 3 concerns the experimental setups used in the study. The conditions of experiment cases are described.

The results of experiment and theoretical simulation are presented in Chapter 4. The properties of TLD are discussed on the basis of the experimental results. The proposed model is verified by comparing with the experiment.

In Chapter 5, several basic parameters affecting the effectiveness of TLD are discussed. The experimental investigations on liquid damping, a most significant parameter of TLD, are presented. Finally in this chapter, an approach for modifying the TLD model for accounting for breaking waves is proposed and verified by the experiment.

Chapter 6 discusses the properties of multiple TLD and the conclusions of the whole study are presented in Chapter 7.

CHAPTER 2 THEORETICAL MODELLING OF WAVE SLOSHING IN TLD

2.1 LINEAR WAVE THEORY

Linear theories on wave motions are herein reviewed for the aim to understand the basic properties of liquid sloshing in TLD, such as natural frequency, pressure distribution, and dispersion relation, etc..

2.1.1 Linear Shallow Water Wave Theory

Considering a 2-dimensional wave fluid as shown in Fig. 2.1 (x-o-z plane), liquid depth is h, and $z=0$ is at the still liquid surface. η describes the free surface elevation, which is a function of location x and time t. L and H express wave length and wave height, respectively. The wave amplitude is assumed to be infinitesimally small, so that the wave motions can be regarded as linear.

Liquid motion is assumed to be inviscid, irrotational, and incompressible. The velocity potential Φ, therefore, exists and is satisfied to Laplace equation, i.e.,

$$\frac{\partial^2 \Phi}{\partial x^2} + \frac{\partial^2 \Phi}{\partial z^2} = 0 . \tag{2.1}$$

Figure 2.1 Definition Sketch for Wave Motion.

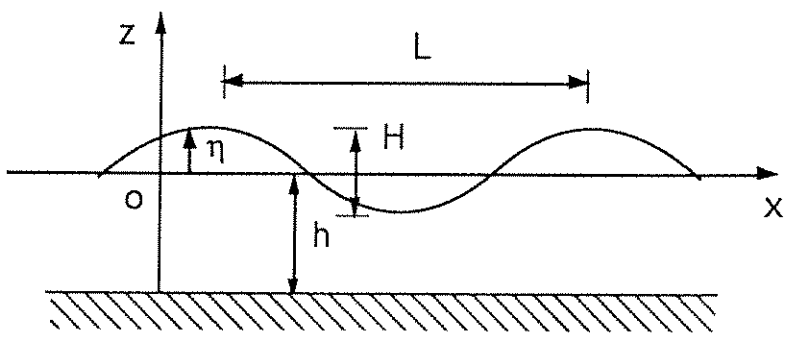

Φ is a function of location (x,z) and time t. This equation should be solved under the boundary conditions. Assuming that velocity potential Φ can be written in the form of

$$\Phi(x,z,t) = X(x)\, Z(z)\, e^{-i\omega t}, \tag{2.2}$$

where $\omega = 2\pi f = 2\pi/T$ is the angular frequency of wave motion, and f and T are the natural frequency and the natural period of wave motion, respectively.

Introducing Eq.(2.2) into Eq.(2.1), the first term is a function of x only, and 2nd one is a function of z only, so it can be written as

$$\frac{\partial^2 X}{\partial x^2} = -\frac{\partial^2 Z}{\partial z^2} \equiv -k^2. \tag{2.3}$$

The solutions to X and Z are assumed to be

$$\begin{aligned} X(x) &= Ae^{ikx} + Be^{-ikx}, \\ Z(z) &= Ce^{kz} + De^{-kz}\ . \end{aligned} \tag{2.4a,b}$$

The coefficients, A, B, C, and D will be determined by the boundary conditions.

The boundary condition at the bottom is

$$w = \frac{\partial \Phi}{\partial z} = 0 \qquad (z = -h). \tag{2.5}$$

Substituting Eqs.(2.4b) and (2.5) into Eq.(2.3), one obtains

$$Z(z) = 2Ce^{-kh}\ \cosh(k(z+h))\ . \tag{2.6}$$

On the free surface $z = \eta(x,t)$, there are two kinds of boundary conditions; one is the dynamical boundary condition

$$p = p_o \equiv 0 \qquad (z = \eta)\ ; \tag{2.7}$$

and the other is the kinematic boundary condition

$$\frac{D\eta}{Dt} \equiv \frac{\partial \eta}{\partial t} + u\frac{\partial \eta}{\partial x} = w \qquad (z = \eta)\ , \tag{2.8}$$

where p_o is the pressure on the free surface. Bernoulli equation expressed as the potential function Φ is given by

$$\frac{\partial \Phi}{\partial t} = \frac{1}{2}\{ (\frac{\partial \Phi}{\partial x})^2 + (\frac{\partial \Phi}{\partial z})^2 \} + \frac{p}{\rho} + g\eta = const\ , \tag{2.9}$$

where ρ is the density of liquid and g is the gravity acceleration. Note $p=p_0=0$ (Eq(2.7)) at the surface. Since the wave amplitude is small, nonlinear terms can be omitted. Hence we obtain

$$\eta \cong -\frac{1}{g}(\frac{\partial \Phi}{\partial t})_{z=\eta} \cong -\frac{1}{g}(\frac{\partial \Phi}{\partial t})_{z=0} . \tag{2.10}$$

On the other hand, omitting second order term from Eq.(2.8), we have

$$\frac{\partial \eta}{\partial t} = \frac{\partial \Phi}{\partial x} \qquad (z = 0) . \tag{2.11}$$

Eliminating η from Eqs.(2.10) and (2.11), the boundary conditions on the free surface are compiled as

$$\frac{\partial^2 \Phi}{\partial t^2} + g\frac{\partial \Phi}{\partial z} = 0 \qquad (z = 0) . \tag{2.12}$$

Introducing Eqs.(2.2), (2.4a) and (2.6) into the above equation leads to

$$\omega^2 = gk\ tanh(kh) . \tag{2.13}$$

Eq. (2.13) is the dispersion relation, and will be discussed later.

Let η take the form of

$$\eta = \frac{H}{2} sin(kx-\omega t) , \tag{2.14}$$

Substituting Eqs.(2.2), (2.4a) and (2.6) into Eq.(2.10) and comparing Eq.(2.14) with Eq.(2.10), the coefficients in Eq.(2.4) can be determined as

$$\begin{matrix} B = 0 \\ 2ACe^{-kh} = -\frac{gH}{2\omega}\frac{1}{cosh(kh)} \end{matrix} . \tag{2.15}$$

Therefore, the velocity potential, Φ can be expressed as

$$\Phi(x,z,t) = -\frac{gH}{2\omega}\frac{cosh\ (k(z+h))}{cosh(kh)} cos\ (kx-\omega t) . \tag{2.16}$$

Note that the profile of Φ along z direction is a function of $cosh(k(z+h))$.

With the aids of Eqs., (2.9) and (2.16), the pressure distribution is expressed as

$$p(x,z,t) = -\rho g \left(z - \frac{\cosh\ (k(z+h))}{\cosh(kh)}\eta\right) . \tag{2.17}$$

2.1.2 Linear Natural Frequency of Liquid Sloshing in a Rectangular Tank

The rigid rectangular tank (Fig. 2.2) which has a length $2a$ and the mean liquid depth h, is subjected to a horizontal motion x_S. The local Cartesian coordinate system (o-x-z) is attached to the tank, and its origin is placed at the center of the mean liquid surface.

For the liquid sloshing in this rectangular tank, the boundary conditions on side walls are

$$u = \frac{\partial \Phi}{\partial x} = 0 \qquad (x=\pm a). \tag{2.18}$$

Since the walls of tank are vertical, the liquid sloshing in a tank can be regarded to be the superposition of a progressing wave and its reflection wave, which have opposite phase and moving in opposite directions. Eqs.(2.14) gives the solution as

$$\begin{aligned} \eta &= \frac{H}{2}\{\sin(kx+\omega t) - \sin(kx-\omega t)\} \\ &= H\cos(kx)\sin(\omega t) \ . \end{aligned} \tag{2.19}$$

Figure 2.2 Definition Sketch for Liquid Sloshing in Rectangular Tank Under Horizontal Motion.

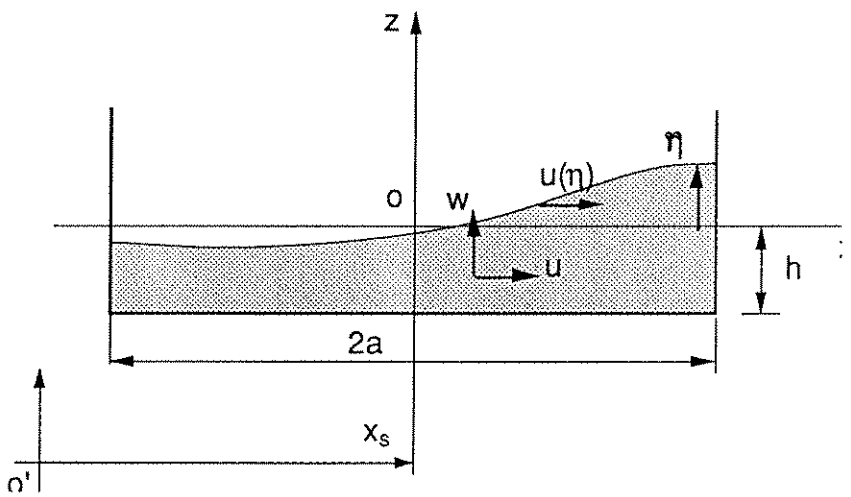

In the case of TLD subjected to a horizontal base motion, unsymmetrical sloshing modes are only excited. So under the coordinate system shown in Fig. 2.2, η takes the form of

$$\eta = H \sin(kx) \sin(\omega t) \ . \tag{2.20}$$

Corresponding to this, velocity potential Φ is rewritten as

$$\Phi(x,z,t) = \frac{gH}{\omega} \frac{\cosh\ (k(z+h))}{\cosh(kh)} \sin(kx)\ \cos(\omega t) \ . \tag{2.21}$$

To satisfy the boundary condition, Eq.(2.18), letting

$$\cos(kx) = 0 \qquad (x = \pm a) \ , \tag{2.22}$$

and

$$k = \frac{2n\text{-}1}{2a} \pi \qquad (n=1,2,.....) \ . \tag{2.23}$$

k is wave number, and can be expressed by a wave length L as

$$k \equiv \frac{2\pi}{L} . \tag{2.24}$$

Note that the wave length of fundamental sloshing mode is 2 times of the length of the tank, i.e., $L=4a$.

Eq.(2.13), that is note that the wave length of fundamental sloshing mode is 2 times of the tank,i.e., L=4a.

$$\omega^2 = gk\ \tanh(kh) \ ,$$

shows the relation between wave frequency and wave number, which is called the dispersion relation, indicating that waves with various wave lengths have different frequencies and travel with different phase velocities.

The natural frequency of liquid sloshing in a rectangular tank is

$$f_n = \frac{\omega_n}{2\pi} = \frac{1}{2\pi} \sqrt{\frac{2n\text{-}1}{2a}\pi g\ \tanh(\frac{2n\text{-}1}{2a}\pi h)} \qquad (n=1,2,.....) \ , \tag{2.25}$$

where n denotes the various modes of liquid sloshing. The fundamental natural frequency (n=1) is

$$f = \frac{\omega}{2\pi} = \frac{1}{2\pi} \sqrt{\frac{\pi g}{2a}\ \tanh(\frac{\pi h}{2a})} \ . \tag{2.26}$$

This formula is employed throughout the thesis for computing the fundamental natural frequency of liquid sloshing in TLD.

2.1.3 Deep Water Wave, Shallow Water Wave and Long Wave

In previous sub-sections, the properties of shallow water wave which is sensitive to the liquid depth have been discussed. There are two extreme situations, i.e., liquid depth h is much larger or much smaller than wave length L. Usually the former is called deep water wave (or surface wave) and the latter long wave (or very shallow water wave). In general, waves in the ranges of $h/L>1/2$ and $h/L<1/20$-$1/25$ are considered to be deep water wave and long wave, respectively (Table 2.1).

Table 2.1 Classification of Waves

h/L	1/20-1/25		1/2
wave type	long wave (very shallow water wave)	shallow water wave	deep water wave (surface wave)
control parameters	h, H/h	H/h, H/L	H/L, L

For the deep water wave, the natural frequency in Eq.(2.26) can be simplified as

$$\omega = \sqrt{\frac{2\pi g}{L}}, \tag{2.27}$$

which is not dependent upon liquid depth, h.

For the long wave, the natural frequency in Eq.(2.26)is simplified as

$$\omega = \sqrt{g k^2 h} = k\sqrt{g h}, \tag{2.28}$$

Then the wave phase velocity, which is defined as

$$c = \frac{\omega}{k} = \frac{L}{T}, \tag{2.29}$$

is expressed as

$$c \equiv c_o = \sqrt{g h}. \tag{2.30}$$

The wave motion properties are controlled only by the liquid depth h.

2.2 NONLINEAR MODEL BASED ON SHALLOW WATER THEORY (UNDER HORIZONTAL MOTION)

2.2.1 Governing Equations

The full equations which govern the liquid motion are the continuity equation

$$\frac{\partial u}{\partial x} + \frac{\partial w}{\partial z} = 0, \tag{2.31}$$

and the two-dimensional Navier-Stokes equations. $u \equiv u(x,z,t)$, $w \equiv w(x,z,t)$ are the velocities of liquid particle (relative to the tank) in the x- and z-direction, respectively. For liquid having relatively small viscosity, the effect of internal friction in the fluid is appreciable only in the boundary layer formed near the solid boundary (Fig. 2.3). From this , the liquid outside the boundary layer may be considered as potential flow, and the equations of motion become

$$\frac{\partial u}{\partial t} + u\frac{\partial u}{\partial x} + w\frac{\partial u}{\partial z} = -\frac{1}{\rho}\frac{\partial p}{\partial x} - \ddot{x}_s \quad (-(h-h_b) \le z \le \eta), \tag{2.32}$$

$$\frac{\partial w}{\partial t} + u\frac{\partial w}{\partial x} + w\frac{\partial w}{\partial z} = -\frac{1}{\rho}\frac{\partial p}{\partial z} - g \quad (-(h-h_b) \le z \le \eta), \tag{2.33}$$

where g is the gravity acceleration. Inside the bottom boundary layer, the equations of motion are

Figure 2.3 Profile of Liquid Particle Velocity in x-direction Inside and outside Boundary Layer.

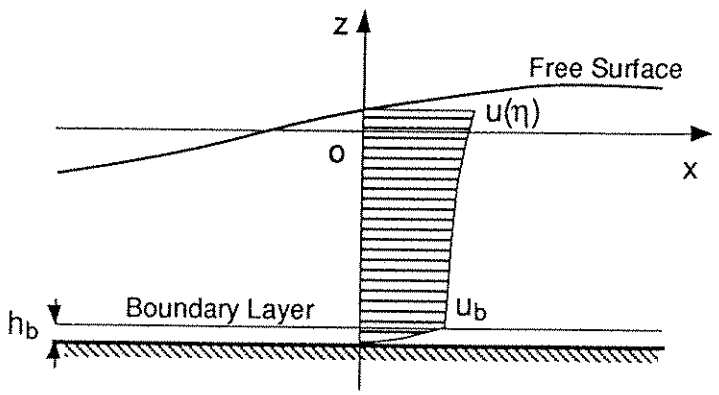

$$\frac{\partial u}{\partial t} + u\frac{\partial u}{\partial x} + w\frac{\partial u}{\partial z} = -\frac{1}{\rho}\frac{\partial p}{\partial x} + \nu\frac{\partial^2 u}{\partial z^2} - \ddot{x}_s \qquad (-h \le z \le -(h-h_b)), \tag{2.34}$$

$$\frac{1}{\rho}\frac{\partial p}{\partial z} = -g \qquad (-h \le z \le -(h-h_b)), \tag{2.35}$$

where h_b is the thickness of boundary layer. This thickness is in the order of several percent of the representative length h in when the liquid in TLD is shallow (Jonsson 1966). ρ and ν are the density and kinematic viscosity of liquid, respectively.

The boundary conditions are

$$u = 0 \qquad \textit{on the end wall } (x = \pm a), \tag{2.36}$$

$$w = 0 \qquad \textit{on the bottom } (z = -h), \tag{2.37}$$

$$w = \frac{D\eta}{Dt} = \frac{\partial \eta}{\partial t} + u\frac{\partial \eta}{\partial x} \qquad \textit{on the free surface } (z = \eta), \tag{2.38}$$

$$p = p_0 = constant \qquad \textit{on the free surface } (z = \eta), \tag{2.39}$$

where D/Dt denotes material differentiation and $\eta \equiv \eta(x,t)$ is the free surface elevation.

2.2.2 Derivations of Basic Equations

The velocity potential function Φ exists for the flow outside the boundary layer. Based on the shallow water wave theory (Eq.(2.16)), Φ may be assumed as (Shimizu and Hayama 1987)

$$\Phi(x,z,t) = \Phi(x,t)\cosh(k(h+z)). \tag{2.40}$$

From Eq.(2.40), the vertical velocity w and its differentials can be expressed in terms of the horizontal velocity u. The equations are integrated with respect to z from bottom to free surface and the basic equations are obtained as

$$\frac{\partial \eta}{\partial t} + h\sigma\frac{\partial(\phi u(\eta))}{\partial x} = 0, \tag{2.41}$$

$$\frac{\partial}{\partial t}u(\eta) + (1-T_H^2)\,u(\eta)\frac{\partial}{\partial x}u(\eta) + g\frac{\partial \eta}{\partial x} + gh\sigma\phi\frac{\partial^2 \eta}{\partial x^2}\frac{\partial \eta}{\partial x} = \frac{\nu}{\eta+h}\int_{-h}^{-(h-h_b)}\frac{\partial^2 u}{\partial z^2}\,dz - \ddot{x}_s, \tag{2.42}$$

where $\sigma=tanh(kh)/(kh)$, $\phi=tanh(k(h+\eta))/tanh(kh)$, $T_H=tanh(k(h+\eta))$, and k is wave number. $u(\eta) \equiv u(x,\eta,t)$ is the horizontal velocity of surface liquid particle. Eq.(2.41) is the integral of the continuity equation while Eq.(2.42) is obtained from the equations of motion after eliminating the pressure p. The independent variables in these basic equations are $u(\eta)$ and η. The first term of the right hand side of Eq.(2.42), which is the integral of the second term of the right hand side of the equation of motion inside the boundary layer (Eq.(2.34)), is referred to as the dissipation term. Details are given in Appendix A.

2.2.3 Damping of Liquid Sloshing

The effect of damping on liquid motion is significant near resonance and hence must be considered carefully in the modelling of the tuned liquid damper. In the present formulation, assuming that the shear stress outside the boundary layer is negligibly small, the dissipation term in Eq.(2.42) can be expressed as

$$\frac{\nu}{\eta+h}\int_{-h}^{-(h-h_b)} \frac{\partial^2 u}{\partial z^2}\,dz = -\frac{1}{(\eta+h)}\frac{1}{\rho}\tau_b, \tag{2.43}$$

where $\tau_b=\rho\nu(\partial u/\partial z)_{z=-h}$, is the bottom shear stress. According to the linear theory of the boundary layer (Lamb 1932), $\tau_b=\sqrt{\omega\nu}\,u(\eta)/\sqrt{2}$, and therefore

$$\frac{\nu}{\eta+h}\int_{-h}^{-(h-h_b)} \frac{\partial^2 u}{\partial z^2}\,dz = -\frac{1}{(\eta+h)}\frac{1}{\sqrt{2}}\sqrt{\omega\nu}\,u(\eta). \tag{2.44}$$

Eq.(2.44) accounts for only the damping effect of bottom boundary layer. Vandorn (1966) reported that the damping of liquid motion in a tank observed from his experiment is larger than that computed only on account of the bottom boundary layer. Miles (1967) also studied the damping of surface wave in closed basin and suggested that the dissipation term should be multiplied by $(1+(2h/b)+S)$, where b is the width of the tank, to account also for dissipation due to side wall friction and liquid surface contamination. It is regarded that the friction of side wall boundary layer is the same as that of bottom boundary layer; $2h/b$ is an equivalent coefficient of the damping effect per unit width due to the side wall boundary layer. S is a "surface contamination" factor which accounts for damping due to stretching effect in the contaminated liquid surface. This can be varied theoretically between 0 and 2 (Miles et al. 1967). A value of unity for S

will be used in this study, which corresponds to the establishment of "fully contaminated surface". Miles et al. (1967) and Lepelletier et al. (1988) also used $S = 1$.

The dissipation term with the inclusion of the effects of side wall and free surface is

$$\frac{\nu}{\eta+h}\int_{-h}^{-(h-h_b)} \frac{\partial^2 u}{\partial z^2}\,dz = -\lambda u(\eta). \tag{2.45}$$

where λ is evaluated as

$$\lambda = \frac{1}{(\eta+h)}\frac{1}{\sqrt{2}}\sqrt{\omega\nu}\,(1+(2h/b)+S)). \tag{2.46}$$

2.2.4 Base Shear Forces due to Liquid Sloshing

Because the liquid is shallow, the pressure p can be expressed from Eq.(2.17) as

$$\frac{1}{\rho}(p-p_0) = g\,(\eta\,\frac{cosh(k(z+h))}{cosh(kh)} - z). \tag{2.47}$$

Integrating Eq.(2.47) with respect to z, the horizontal total pressure P, force acting on the end wall of the TLD tank can be calculated.

Neglecting the frictions of side wall and bottom, the base shear force, $F \equiv F(t)$, of the tank due to liquid motion is

Figure 2.4 Base Shear Force due to Liquid Motion.

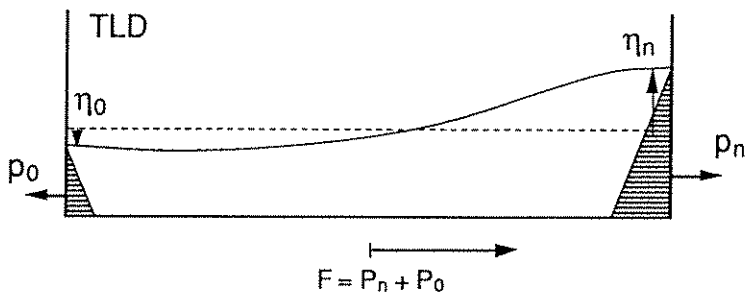

$$F = P_n + P_0. \tag{2.48}$$

P_n and P_0 are the liquid-induced horizontal force (total pressures) acting on the right and left end walls of the tank, respectively (Fig. 2.4). These are functions of liquid free surface elevation at the end walls.

2.2.5 Numerical Solution by Runge-Kutta-Gill Method

The basic equations (Eqs.(2.41) and (2.42)) are discretized with respect to x into difference equations (staggered mesh) and can be solved numerically. The free surface waves originally possess a dispersion character. This is replaced by the dispersion relation, which is produced by the discretization of the basic equations with proper choice of a suitable division number n. The dimensionless wave number is taken as $\pi/(2a)$, since the frequency around the fundamental natural frequency is of main concern. In this paper, n is calculated using (Shimizu and Hayama 1987):

$$n = \pi \,/\, (2arccos(\sqrt{(tanh(\pi\varepsilon)/(2tanh(\pi\varepsilon/2))}) \quad (\varepsilon = h/a). \tag{2.49}$$

After determining the division number n and with the corresponding boundary condition

$$u(\eta) = 0 \qquad (x = \pm a), \tag{2.50}$$

the difference basic equations are solved using Runge-Kutta-Gill method and $u(\eta)$ and η can be computed (Appendix A).

2.3 NONLINEAR MODEL BASED ON SHALLOW WATER THEORY (UNDER PITCHING MOTION)

2.3.1 Inertia Forces in a Rotational Coordination System

As shown in Fig. 2.5, the fixed rectangular coordination is XOZ, and another rectangular coordination system xoz can rotate around the origin O with angular deformation θ. The inertia forces under the system xoz are

$$m\ddot{x} = m (- g \sin\theta + 2\dot{z}\dot{\theta} + x\dot{\theta}^2 + z\ddot{\theta}) \tag{2.53}$$

$$m\ddot{z} = m (- g \cos\theta - 2\dot{x}\dot{\theta} + z\dot{\theta}^2 - x\ddot{\theta}) \tag{2.54}$$

where the 1st term is the effect of gravity; the 2nd term is Coriolis' force; the 3rd term is centrifugal force, and the 4th term is tangent acceleration force [Koga 1990].

Figure 2.5 Inertia Forces in a Rotational Coordination System

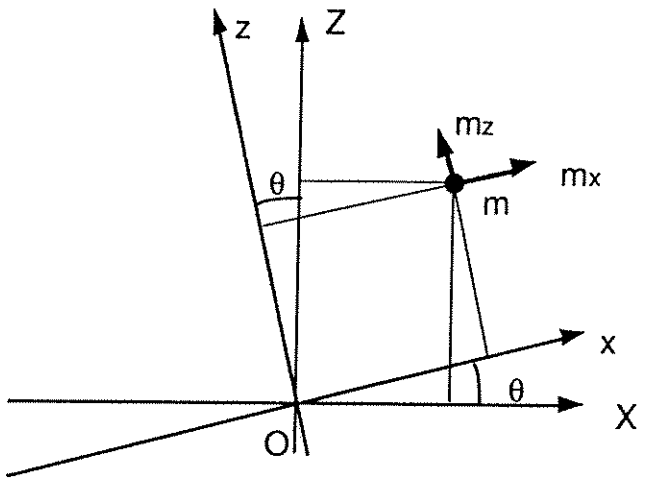

2.3.2 Derivations of Basic Equations

The motion of TLD tank is shown in Fig. 2.6.. The coordination system XOZ is fixed and the another coordination system xoz moves with TLD tank together.. The motion of TLD tank can be expressed by X_o, Z_o, and θ. The assumptions in this section are the same as that in Section 2.2. Therefore, the equations governing the problem are still the equation of continuity:

$$\frac{\partial u}{\partial x} + \frac{\partial w}{\partial z} = 0, \tag{2.55}$$

Equations of motion (Eular's equations):

$$\frac{\partial u}{\partial t} + u\frac{\partial u}{\partial x} + w\frac{\partial u}{\partial z} = -\frac{1}{\rho}\frac{\partial p}{\partial x} - a_x \quad (h_b \le z \le h+\eta), \tag{2.56}$$

$$\frac{\partial w}{\partial t} + u\frac{\partial w}{\partial x} + w\frac{\partial w}{\partial z} = -\frac{1}{\rho}\frac{\partial p}{\partial z} - a_z \quad (h_b \le z \le h+\eta), \tag{2.57}$$

where a_x and a_z are the inertia forces acting on liquid in TLD, and can be expressed under the coordination system shown in Fig. 2.6 as

$$\begin{cases} a_x = -g\sin\theta + 2\dot{\theta}w + \ddot{\theta}z + \dot{\theta}^2 x - \ddot{X}_o\cos\theta - \ddot{Z}_o\sin\theta & (2.58) \\ a_z = -g\cos\theta - 2\dot{\theta}u - \ddot{\theta}x + \dot{\theta}^2 z + \ddot{X}_o\sin\theta - \ddot{Z}_o\cos\theta & (2.59) \end{cases}$$

Figure 2.6 Definition Sketch for Liquid Sloshing in Rectangular Tank Under Pitching Motion.

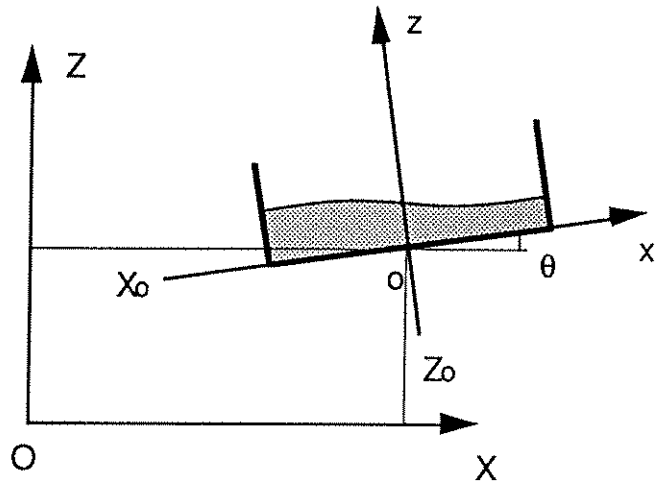

Note that the components of $\ddot{X}_o$ and $\ddot{Z}_o$ are included in a_x and a_z also. Because the liquid depth considered herein is shallow, i.e., the dimension in x-direction is much larger than that in z-direction, the accelerations a_x and a_z can be simplified by neglecting higher order terms. They are rewritten as

$$\begin{cases} a_x \approx -(g + \ddot{Z}_o)\sin\theta + \ddot{\theta}z - \ddot{X}_o\cos\theta & (2.60) \\ a_z \approx -(g + \ddot{Z}_o)\cos\theta - \ddot{\theta}x + \ddot{X}_o\sin\theta & (2.61) \end{cases}$$

The boundary conditions are:

$$u = 0 \qquad (x = \pm a) \qquad (2.62)$$

$$w = 0 \qquad (z = 0) \qquad (2.63)$$

$$w = \frac{\partial \eta}{\partial t} + u\frac{\partial \eta}{\partial x} \qquad (z = h + \eta) \qquad (2.64)$$

$$p = p_o = const. \quad (z = h + \eta) \tag{2.65}$$

The liquid damping is treated in the same way as discussed in Section 2.3. The derivations of basic equations are similar to the approach in Section 2.2, and the details are presented in Appendix C. The basic equations were obtained as

$$\frac{\partial \eta}{\partial t} + h\sigma \frac{\partial(\phi u(\eta))}{\partial x} = 0, \tag{2.66}$$

$$\frac{\partial}{\partial t} u(\eta) + \frac{1}{2}\frac{\partial}{\partial x} u(\eta)^2 + ((g + \ddot{Z}_o)\cos\theta - \ddot{X}_o \sin\theta + \ddot{\theta} x + (g + \ddot{Z}_o)\cos\theta\, h\sigma\phi \frac{\partial^2 \eta}{\partial x^2}) \frac{\partial \eta}{\partial x} = -(g + \ddot{Z}_o)\sin\theta - \ddot{X}_o \cos\theta - \lambda u(\eta). \tag{2.67}$$

2.3.3 Forces and Moments due to Liquid Sloshing

According to Eq.(2.17), the pressure distribution of liquid can be expressed as

$$p - p_o = -\rho a_z \left(h + \frac{\cosh(kz)}{\cosh(kh)} \eta - z \right). \tag{2.68}$$

Because the liquid is shallow,

$$\cosh(kz) \approx \cosh(kh) \approx 1.$$

Figure 2.7 Forces and Moment due to Liquid Sloshing.

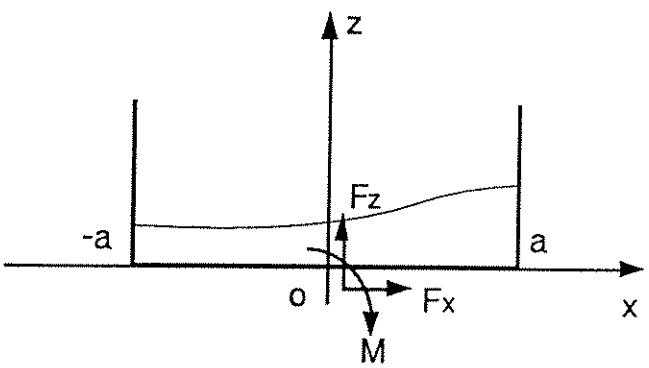

So, the pressure distribution can be described approximately as

$$p - p_o = - \rho a_z (h + \eta - z), \tag{2.68}$$

where p_o is the pressure on the liquid surface and takes a value of 0.

The forces and moments (Fig. 2.7) due to liquid sloshing are

$$F_x = -\frac{1}{2} \rho b a_z ((h+\eta_a)^2 - (h+\eta_{-a})^2); \tag{2.69}$$

$$F_z = \int_{-a}^{a} \rho b a_z (h+\eta) dx \; ; \tag{2.70}$$

$$M = -\frac{1}{6} \rho b a_z ((h+\eta_a)^3 - (h+\eta_{-a})^3) - \int_{-a}^{a} \rho b a_z (h+\eta) x dx \tag{2.71}$$

Note that the moment due to liquid sloshing consists of two parts, namely that due to the horizontal sloshing force acting on the side walls and that due to liquid weight acting on the bottom. Since liquid is shallow ($h/a << 1$), the later is more significant in the moment. The solutions of the basic equations are given in details in App. B.

2.4 NUMERICAL SIMULATION BY USE OF SOLA-VOF CODE

2.4.1 Preliminary Remarks

As the development of computers, especially supercomputers with high CPU speed and large memory, the numerical simulations and numerical experiments on flow are used increasingly. The liquid sloshing without breaking waves were solved by using FEM and BEM [Nakayama 1981]. Recently, Ohyama [1989] proposed a BEM approach to treat the wave motion and the induced hydrodynamic force in TLD.

Viscous liquid sloshing with breaking waves in a rectangular tank is a important phenomenon in TLD. Numerical simulation method for breaking waves have been developed by several researchers [Nichols et al. 1980, Miyata 1987]. SOLA-VOF [Nichols et al. 1980] is one of them and has been reported to be able to treat liquid motion with breaking waves.

SOLA-VOF is a finite difference method. The fractional Volume Of Fluid (VOF) method forms the basis of the SOLA-VOF program. The VOF techniques provides a means of following fluid regions through an Eulerian mesh of stationary cells. In principle, the VOF method could be used to track any surface of discontinuity in material properties, in tangential velocity, or any other property. SOLA-VOF code has a cycle-to-cycle self adjustment technique which can justify the flow flux automatically even if the continuity equation is not satisfied enough in time-marching. We try to use this code to treat liquid sloshing in TLD with breaking wave.

The Outline of SOLA-VOF code is briefly explained. A few test problems have been computed and the results are presented and discussed in section 4.5. It is found, however, that the SOLA-VOF code is not valid for an engineering application.

2.4.2 Outline of SOLA-VOF Code

SOLA-VOF (Solution Algorithm-Volume of Function) has an Eulerian mesh of rectangular cells with variable sizes, as shown in Fig. 2.8, δx_i for the i^{th} column and δz_i for the j^{th} row. The dependent variables, including the fractional volume of fluid F variable used in the VOF technique, are located at cell positions shown in the figure.

Figure 2.8 Location of variables in a typical mesh cell.

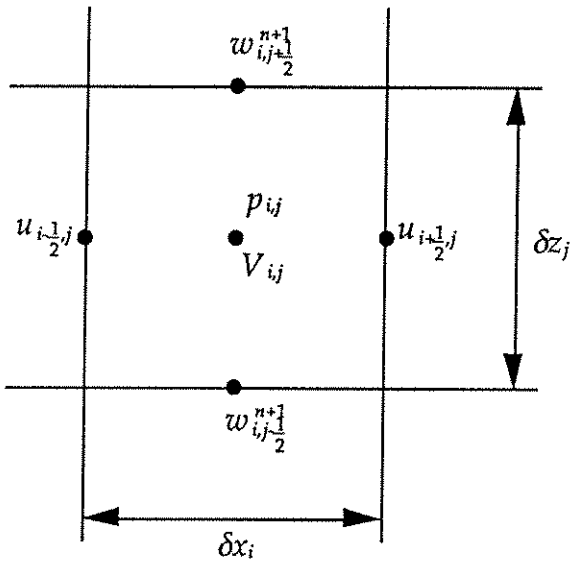

The basis of the SOLA-VOF method is the fractional volume of fluid scheme for tracking free boundaries. In this technique, a function $V(x,y,t)$ is defined whose value is unity at any point occupied by fluid and zero elsewhere. The average value of V in a cell is equal to the fractional volume of the cell occupied by fluid. In particular, a unit value of V corresponds to a cell full of fluid, where as a zero value indicates that the cell contain no fluid. Cells with V values between zero and one contain a free surface.

The equations to be solved are continuity equation and Navier-Stokes equations. The volume of fluid function V is used to identify mesh cell that contain fluid of density ρ. A free surface cell (i,j) is defined as a cell containing a nonzero of V and having at least one neighboring cell $(i\pm1,j)$ or $(i,j\pm1)$ that contains a zero value of V. Cells with zero V values are empty of contain material of density ρ_c.

In the following, the notation $Q_{i,j}$ stands for the value of $Q(x,z,t)$ at the $n\delta t$ and at a location (i,j). Half integer subscripts refer to cell boundary locations.

A generic form for the finite-difference approximation of Navier-Stokes equations is

$$u_{i+\frac{1}{2},j}^{n+1} = u_{i+\frac{1}{2},j}^{n} + \delta t \left[- (p_{i+1,j}^{n+1} - p_{i,j}^{n+1}) / \delta\rho x_{i+\frac{1}{2}} + \ddot{x}_s - FUX - FUZ + VISX \right] \qquad (2.72)$$

and

$$w_{i,j+\frac{1}{2}}^{n+1} = w_{i,j+\frac{1}{2}}^{n} + \delta t \left[- (p_{i,j+1}^{n+1} - p_{i,j}^{n+1}) / \delta\rho z_{j+\frac{1}{2}} + g - FWX - FWZ + VISZ \right] \qquad (2.73)$$

where

$$\delta\rho x_{i+\frac{1}{2}} = \frac{1}{2} \{ [\rho_c + (\rho - \rho_c) V_{i,j}] \delta x_{i+1} + [\rho_c + (\rho - \rho_c) V_{i+1,j}] \delta x_i \qquad (2.74)$$

and

$$\delta\rho z_{j+\frac{1}{2}} = \frac{1}{2} \{ [\rho_c + (\rho - \rho_c) V_{i,j}] \delta z_{j+1} + [\rho_c + (\rho - \rho_c) V_{i,j+1}] \delta z_j. \qquad (2.75)$$

The advective and viscous acceleration terms have an obvious meaning, e.g., FUX means that advective flus of u in x-direction, etc..

Velocities computed from Eqs.(2.72) and (2.73) must satisfy the continuity equation. In order to satisfy this equation, the pressures (and velocities) must be

adjusted in each cell occupied by fluid. Assuming that introduction of velocities $\tilde{u}$ and $\tilde{w}$ computed from Eqs.(2.72) into Eq.(2.73) causes a error ΔS

$$\Delta S = \frac{\partial \tilde{u}}{\partial x} + \frac{\partial \tilde{w}}{\partial z}. \tag{2.76}$$

ΔS is a function of pressure p and should be made to be zero by modifying p:

$$\Delta S(p+\delta p) = 0. \tag{2.77}$$

Make a Taylar expansion of the above equation and omit the higher order terms, δp is obtained as

$$\delta p = -\Delta S \,/\, (\frac{\partial \Delta S}{\partial p}). \tag{2.78}$$

The new estimate for the pressure of cell (i,j) is then

$$p_{i,j} + \delta p\,, \tag{2.79}$$

and new estimates for the velocities locates on the side of the cell are

$$u_{i+\frac{1}{2},j} + \delta t\ \delta p \,/\, \delta \rho x_{i+\frac{1}{2}}; \tag{2.80}$$

$$u_{i-\frac{1}{2},j} - \delta t\ \delta p \,/\, \delta \rho x_{i-\frac{1}{2}}; \tag{2.81}$$

$$w_{i,j+\frac{1}{2}} + \delta t\ \delta p \,/\, \delta \rho z_{j+\frac{1}{2}}; \tag{2.82}$$

$$w_{i,j-\frac{1}{2}} - \delta t\ \delta p \,/\, \delta \rho z_{j-\frac{1}{2}}; \tag{2.83}$$

Briefly, the basic procedure for advancing a solution through one increment in time, δt, consists of three steps:

(1) Semi-implicit approximations of Eq.(2.72) and Eq.(2.73) are used to compute the first guess for new time-level velocities using the initial conditions or previous time-level values for all advective pressure, and viscous accelerations.

(2) To satisfy the continuity equation, Eq.(2.31), pressures are iteratively adjusted in each cell and the velocity changes induced by each pressure change are added to the velocities computed in step (1). An iteration is needed because the change in pressure needed in one cell to satisfy Eq.(2.77) will upset the balance in the four adjacent cells.

(3) Finally, the V function defining fluid regions must be updated to give the mew fluid configuration.

Repetition of these steps will advance a solution through any desired time interval. At each step, of corse, suitable boundary conditions must be imposed at all mesh and free-surface boundaries. The details of SOLA-VOF method are given in Nichols' paper [1980].

2..5 MODIFICATION OF BASIC EQUATIONS FOR BREAKING WAVES

In practice, plain water is usually used as liquid in TLD. It gives, however, rather low liquid damping compared with the optimal value. A few means were reported to increase liquid damping; among those, the utilizing of shallow liquid is one of the easy choices. The problem with shallow liquid, however, is the presence of breaking waves.

The TLD model proposed is not valid for wave breaking situation because of the assumption of free surface continuity. To account for breaking waves in the TLD model, the equation of motion (Eq.(10)) was modified by introducing two coefficients, C_{da} and C_{fr} as follows,

$$\frac{\partial u(\eta)}{\partial t} + (1-T_{\bar{n}}^2)\, u(\eta)\frac{\partial u(\eta)}{\partial x} + C_{fr}^2\, g\frac{\partial \eta}{\partial x} + gh\sigma\phi\frac{\partial^2\eta}{\partial x^2}\frac{\partial \eta}{\partial x} = -C_{da}\lambda u(\eta) - \ddot{x}_s. \qquad (2.52)$$

Those coefficients are unity when breaking waves do not exist. Referring to the definition of breaking waves in coastal engineering, the critical condition of breaking waves in this study is defined as that wave height is larger than liquid depth h.

When waves break, more energy will be dissipated on the liquid free surface, indicating that liquid sloshing has higher damping. Therefore, C_{da} was introduced in Eq.(15) to modify the liquid damping, and is called as a damping coefficient. On the other hand, wave breaking will also change correspondingly the wave phase velocity. So, C_{fr} was introduced into Eq.(15) to modify the phase velocity. As the change of wave phase velocity also reflects the shift of the natural frequency of liquid sloshing, C_{fr} is called as a frequency shift coefficient.

Values of these two empirical coefficients were identified by the sweep harmonic shaking table experiment as described in Section 5.4.

2.6 TLD-STRUCTURE INTERACTION

2.6.1 Interaction Model Under Horizontal Motion

TLD-structure interaction model, which consists of a linear single-degree-of-freedom (SDOF) structure and an attached TLD (Fig. 2.9), can be used to simulate the response of the structure with attached TLD.

Figure 2.9 TLD-Stucture Interaction under Horizontal Motion.

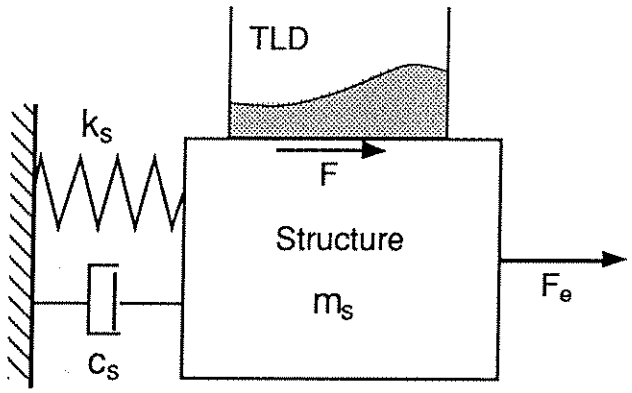

The equation of motion of the structure, which subjects to sinusoidal external force $F_e = F_{eO} \sin\omega t$ and to TLD base shear force F, can be expressed as

$$\ddot{x}_s + 2\omega_s \xi_s \dot{x}_s + \omega_s^2 x_s = \frac{1}{m_s}(F + F_e) \tag{2.84}$$

where $\omega_s = \sqrt{(k_s / m_s)}$, is the undamped natural frequency of the structure; ξ_s is the structural damping ratio; m_s is the mass of structure. TLD base shear force F is determined by Eq.(2.48). Accordingly, at each time step in the numerical simulation, x_s, η and $u(\eta)$ are computed simultaneously from the three coupled equations (Eqs. 2.41, 2.42 and 2.84).

2.6.2 Interaction Model Under Pitching Motion

The equation of motion for a TLD-structure system under pitching motion (Fig. 2.10) is expressed as

$$\ddot{\theta}_s + 2\omega_s\xi_s\dot{\theta}_s + \omega_s^2\theta_s = (M + M_e)/I_s, \tag{2.86}$$

where θ_s is the rotational displacement of structure and I_s is the moment of inertia to O. M_e is external moment. M is the moment acting on structure due to the liquid motion in TLD (Eq. 2.70). Solving the simultaneous equations of Eq.(2.86) and governing equation of liquid motion (Eqs,(2.66) and (2.67)), the response of the structure with TLD under pitching motion can be obtained.

Figure 2.10 TLD-Stucture Interaction under Pitching Motion.

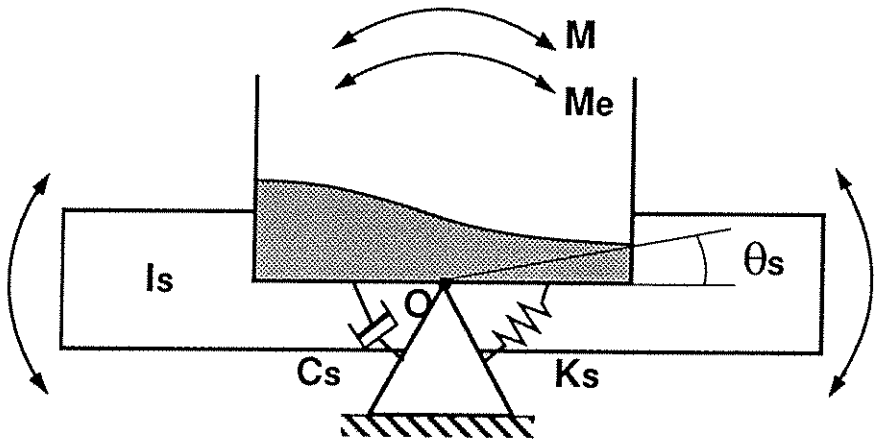

CHAPTER 3 EXPERIMENTAL APPARATUS AND PROCEDURES

In this study, two types of experiments were carried out, namely, the shaking table experiment of TLD under horizontal motion or pitching motion; and the experiment of TLD-structure interaction, in order to assess the validity of the proposed TLD models and to study the properties of liquid sloshing in TLD as well as the effectiveness of TLD.

The set-ups and the experimental cases are described in this chapter and the results of the experiments will be presented and discussed in Chapter 4.

3.1 SHAKING TABLE EXPERIMENT UNDER HORIZONTAL MOTION

3.1.1 Experimental Set-up

A shaking table was employed in the experiment. This can generate a steady harmonic horizontal motion with a frequency in the range of *0.1-700 Hz* and a amplitude up to *4.0 cm*. Both the excitation frequency and the amplitude are

Figure 3.1 The Setup of Shaking Table Experiment (Horizontal Motion).

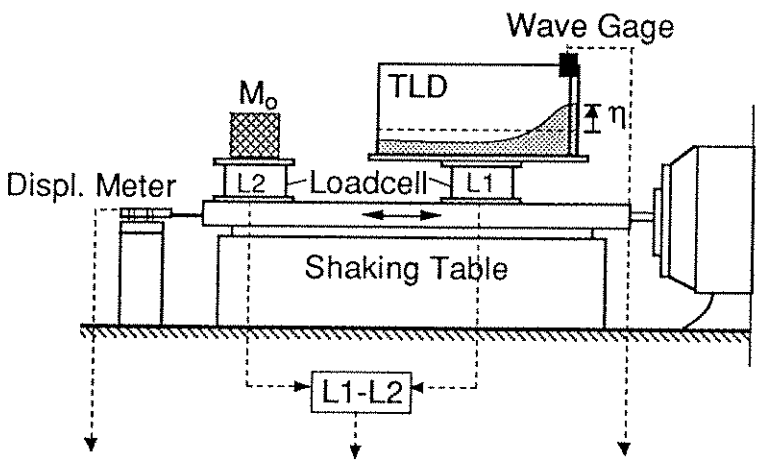

adjustable manually. The rectangular TLD tank was excited horizontally by this shaking table (Fig. 3.1).

A capacitance wave gage was installed at the end wall of the TLD tank to measure the liquid surface elevation. To measure the base shear force of TLD tank induced purely by liquid sloshing, two load cells L1 and L2 were used. L1 was installed in the base of TLD to measure the base shear force in which the inertia force of TLD tank was included. Another load cell L2 was installed in a dummy mass M_0 which is equal to that of TLD tank to measure its inertia force. The difference between L1 and L2, i. e., the base shear force purely due to liquid sloshing in TLD, was obtained by a shift amplifier. The displacement of the shaking table was recorded by a displacement meter.

In the experiment, the TLD was initially quiescent and was excited sinusoidally with constant amplitude at each excitation frequency. The experimental data were processed by a NEC micro computer.

3.1.2 Experimental Cases

First, a group of cases were carried out to assess the proposed TLD model and investigate the characteristics of TLD, such as nonlinearities, etc..

A rectangular tank with length $2a = 59.0\ cm$ (measured along the direction of excitation) and width $b = 33.5\ cm$, being made of $0.5\ cm$ thick acrylic plates was

Figure 3.2 TLD Tank.

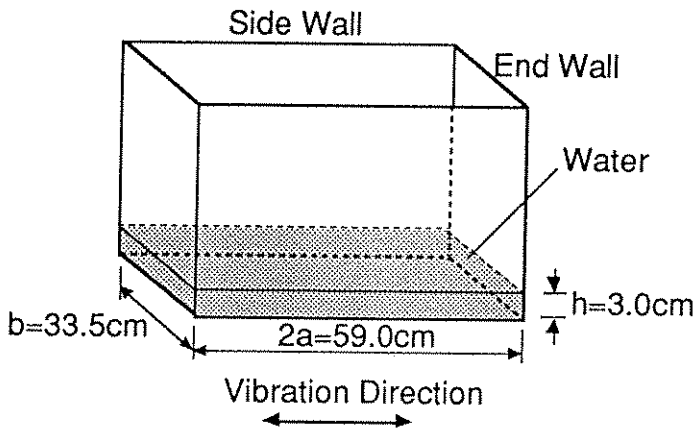

used (Fig. 3.2). The TLD tank was partially filled with plain water of $h = 3.0\ cm$ depth, corresponding to liquid depth ratio $\varepsilon = h/a = 0.1$. Water mass m_w is $5.93\ kg$. From the linear wave theory, the fundamental natural frequency of liquid sloshing motion, f_w, is

$$f_w = \frac{1}{2\pi}\sqrt{\frac{\pi g}{2a}\tanh(\frac{\pi h}{2a})} = 0.458\ Hz,$$

i.e., the natural period was $T_w = 2.18\ sec$. For four amplitudes of displacement of shaking table, $A = 0.1\ cm, 0.25\ cm, 0.5\ cm$, and $1.0\ cm$, the excitation frequency f was varied in the range of $0.8 < f/f_w < 1.3$.

Table 3.1 Shaking table experiment cases for verifying proposed TLD model.

Case name	Tank size (cm) Length $2a$ (cm)	Width b (cm)	Liquid depth h (cm)	Depth ratio $\varepsilon=h/a$	Natural freq. f_w (Hz)	Excitation amp A (cm)
6N1-01	59.0	33.5	3.0	0.1	0.458	0.1
6N1-025	59.0	33.5	3.0	0.1	0.458	0.25
6N1-05	59.0	33.5	3.0	0.1	0.458	0.5
6N1-10	59.0	33.5	3.0	0.1	0.458	1.0

Next, a group of cases was carried out to identified two empirical coefficients for liquid sloshing with breaking waves as described in sub-section 2.2.5. Two types of TLD tank was used and the excitation amplitude was relatively large and breaking waves occurred in TLD. The case are shown in Table 3.2.

Table 3.2 Shaking table experiment cases for determining C_{da} and C_{ft}

Case name	Tank size (cm) Length $2a$ (cm)	Width b (cm)	Liquid depth ratio $\varepsilon=h/a$	Natural freq. f_w (Hz)	Excitation amp. A (cm)
4N1	39.0	22.0	0.1	0.565	0.1 ~ 4.0
4N2	39.0	22.0	0.2	0.789	0.1 ~ 4.0
6N1	59.0	33.5	0.1	0.458	0.1 ~ 4.0
6N2	59.0	33.5	0.2	0.639	0.1 ~ 4.0

Then the experiments using TLD with various liquid depth were carried out to investigate the effect of liquid depth ratio (Table 3.3).

Table 3.3 Shaking table experiment cases for studying effects of liquid depth ratio.

Case name	Tank size (cm) Length $2a$ (cm)	Width b (cm)	Liquid depth h (cm)	Depth ratio $\varepsilon=h/a$	Natural freq. f_w (Hz)	Excitation amp. A (cm)
6W2A	59.0	33.5	6.0	0.2	0.639	0.1
6W4A	59.0	33.5	12.0	0.4	0.864	0.1
6W6A	59.0	33.5	18.0	0.6	0.992	0.1
6W8A	59.0	33.5	24.0	0.8	1.064	0.1

The experiments were also carried out for investigating the damping effects of liquid sloshing by using high viscous-liquid (Table 3.4), and by adding floating materials on the free surface (Table 3.5).

Table 3.4 Shaking table experiment cases for studying damping effects of liquid viscosity.

Case name	Tank size (cm) Length $2a$ (cm)	Width b (cm)	Liquid depth ratio $\varepsilon=h/a$	Viscosity ratio ν/ν_w	Natural freq. f_w (Hz)	Excitation amp. A (cm)
6V11	59.0	33.5	0.1	11.2	0.458	0.5
6V30	59.0	33.5	0.1	30.0	0.458	0.5

Table 3.5 Shaking table experiment cases for studying damping effects of floating materials.

Case name	Tank size (cm) Length $2a$ (cm	Width b (cm)	Liquid depth ratio ε	Volume of materials (cc)	Natural freq. f_w (Hz)	Excitation amp. A (cm)
6T05	59.0	33.5	0.2	500	0.639	1.0
6T10	59.0	33.5	0.2	1000	0.639	1.0

3.2 SHAKING TABLE EXPERIMENT UNDER PITCHING MOTION

3.2.1 Experimental Set-up

In order to assess the validity of the simulation results, and investigate the properties of liquid motion in TLD subjected to pitching motion in vertical plane, the experiments were carried out.

A shaking table which can rotate in vertical plane was designed. This consists of a beam, a spring and a exciter. As shown in Fig. 3.3, the beam is supported by a hinge at one end, and is suspended by a spring at the other end, where a exciter is mounted to generate vertical motion. A function generator was used to generate a sinusoidal signal, and this was amplified by a power amplifier. Inputing the amplified signal into the exciter, the moving part of exciter can oscillate sinusoidally. The oscillation frequency and amplitude can be controlled easily. TLD tank is placed on the beam at the pin point, where the beam is able to rotate owing to the vertical motion of the other end of the beam.

The moving part of the exciter generates the inertia force, which is employed as the excitation force to excite the beam rotationally. The force can be adjusted by changing amplitude or mass of the moving part of the exciter. Because the power

of the exciter is rather low, the natural frequency of the beam was designed to lie in the range of sweep frequency so that a large enough amplitude can be obtained. The natural frequency of the beam was adjusted at about *0.5 Hz* in the experiment. However, since the damping of the beam was quite low, the amplitude of the beam was very sensitive to the excitation frequency and the beating response was observed at some frequencies. As a result, it is quite difficult to keep the amplitude of the beam constant in full range of the sweep test. Furthermore, the exciter used in the experiment did not generate purely sinusoidal motion when the oscillation frequency is lower than *1.0 Hz*.

A capacity wave gage was used to measure the free surface elevation near the wall of TLD tank. The displacement of the beam was measured by a position sensor, from which the rotational angle of TLD θ_o can be known.

Figure 3.3 Setup of Shaking Table Experiment (Pitching Motion)

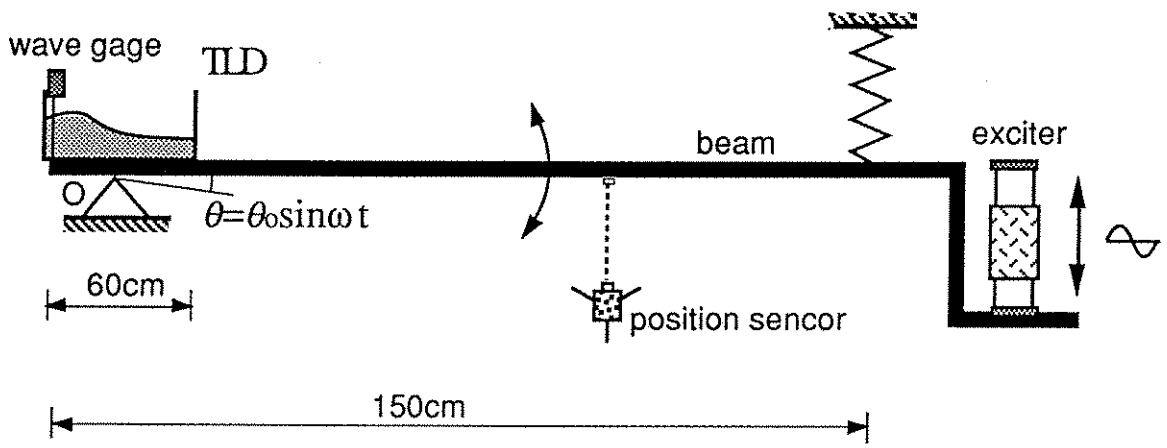

3.2.2 Experimental Cases

TLD tank used is the same as described in Section 3.1. Water was used as liquid in TLD, liquid depth h is *3 cm* and *4 cm*. The depth ratio h/a are *0.10* and *0.13*, corresponding to the natural frequencies are f_w=*0.458 Hz* and *0.527 Hz*, respectively. So the liquid motion can be treated as shallow wave.

During the experiment, the TLD was excited by a sinusoidal pitching motion with constant amplitude. The excitation frequency was varied around the

resonant frequency of liquid sloshing. The excitation amplitudes were θ_0=0.1 *deg* , 0.2 *deg* and 0.3 *deg* for the case h=3.0 *cm* and θ_0=0.1 *deg* for the case h=4.0 *cm*. For all of the cases, the excitation frequency f varied in the range of $0.8<f/f_w/1.2$. (Table 3.6).

Table 3.6 Shaking table experiment cases for verifying the proposed TLD model (Pitching Motion).

Case name	Tank size (cm)		Liquid depth	Depth ratio	Natural	Excitation angle
	Length $2a$ (cm)	Width b (cm)	h (cm)	$\varepsilon=h/a$	freq. f_w (Hz)	Θ (deg)
R6N1-01	59.0	33.5	3.0	0.1	0.458	0.1
R6N1-02	59.0	33.5	3.0	0.1	0.458	0.2
R6N1-03	59.0	33.5	3.0	0.1	0.458	0.3
R6N2-01	59.0	33.5	4.0	0.133	0.527	0.1

3.3 TLD-STURCTURE INTERACTION EXPERIMENT

3.3.1 Experimental Set-up

The structure model used in the interaction experiment was a SDOF platform vibrating horizontally in a shear-type motion (Fig.3.4) and its natural frequency

Figure 3.4 Setup of TLD-structure interaction experiment (Horizontal motion).

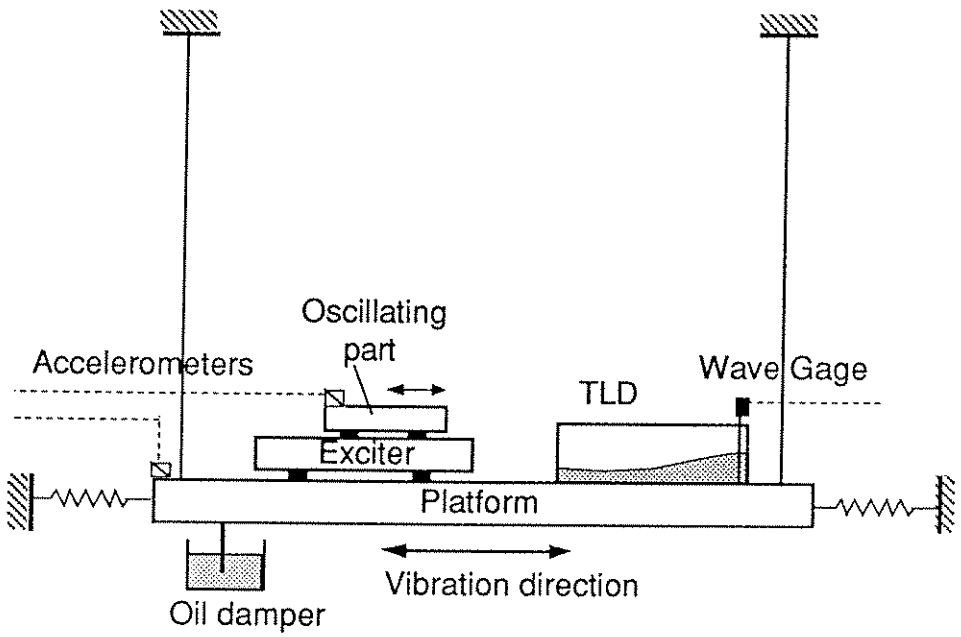

can be adjusted by changing the mass of platform or the stiffness of springs. The damping of the platform is controlled by a oil damper. TLD was mounted on the platform. The external sinusoidal force exerted to the structure was the inertia force of the moving part of an exciter which was mounted horizontally on the platform. The external force amplitude was accordingly maintained constant by keeping constant the amplitude of relative acceleration of the oscillating part to the platform. Sweep of excitation frequency, f was done and the steady-state structural response and the liquid surface elevation near the end wall of TLD tank were measured.

3.3.2 Experimental Cases

Two TLD-structure interaction experiment cases shown in Table 3.7 were carried out by Chaiseri [1990]. These two cases were referred to compare with numerical simulations. The structural mass ms is *168 kg*, and the natural frequency of structure, f_s is *0.91 Hz* (the natural period T_s = *1.10 sec*). The damping ratio of the structure model is *0.32%* (corresponding to the logarithmic damping δ_s of *0.02* The constant amplitude of exciting force for that frequency range, was selected such that the structure without TLD vibrated at the steady-state amplitude A_o at resonance. A rectangular tank with water was used as TLD. Water depth h in TLD was determined such that the fundamental natural frequency of sloshing motion was tuned to the structural natural frequency. The mass ratio of water to that of the structure is μ.

Table 3.7 TLD-structure interaction experiment cases (without breaking waves).

	Structure				TLD Tank			
Case name	fs (Hz)	δs	Ao (cm)	μ(%)	2a (cm)	b (cm)	h (cm)	f_w (Hz)
TS251	0.90	0.02	1.0	1.00	25.0	32.0	2.1	0.90
TS321	0.90	0.02	3.0	0.87	32.0	25.0	3.6	0.90

Additional experimental cases were carried out to assess the modified TLD model accounting for breaking waves. The resonance amplitude of structures in these cases are relatively large and the breaking waves are expected to occur. The cases are shown in Table 3.8.

Table 3.8 TLD-structure interaction experiment cases (with breaking waves).

	Structure				TLD Tank			
Case name	fs (Hz)	δs	Ao (cm)	μ(%)	2a (cm)	b (cm)	h (cm)	f_w (Hz)
TS405	1.45	0.02	5.0	1.05	39.0	22.0	3.0	1.45
TS410	1.45	0.02	10.0	1.05	39.0	22.0	3.0	1.45

CHAPTER 4 PRESENTATIONS AND DISCUSSIONS OF EXPERIMENTAL AND THEORETICAL RESULTS

4.1 DEFINITIONS OF QUANTITIES FOR PRESENTATIONS

Figure 4.1 shows sample time histories of displacement of shaking table, x_s; liquid free surface elevation at the end wall, η_o; and base shear force, F, with liquid sloshing at steady state in the horizontal shaking table experiment. Several quantities are defined as follows for the presentations of results.

Figure 4.1 Sample time histories of displacement of shaking table, x_s, liquid surface elevation near the end wall, η_o and base shear Force, F (Shaking table experiment under horizontal motion).

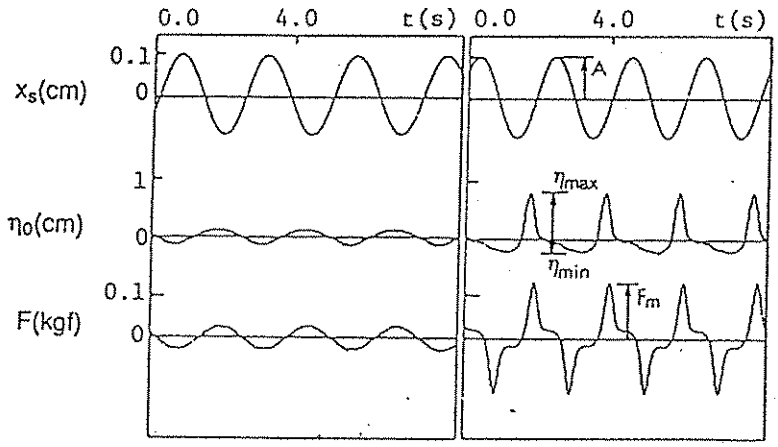

(a) A=0.1cm, f/f_w=0.90 (b) A=0.25cm, f/f_w=1.06

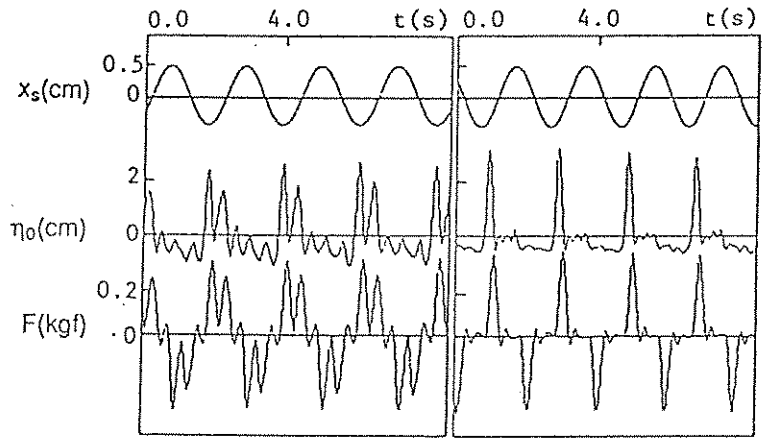

(c) A=0.5cm, f/f_w=1.06 (d) A=1.0cm, f/f_w=1.14

Dimensionless Maximum and Minimum Liquid Surface Elevation at the End Wall of TLD Tank. Liquid free surface elevation at the end wall of TLD tank, η_o equals 0 at still liquid free surface. During liquid sloshing, η_o has a maximum value η_{max} (wave crest) and a minimum value η_{min} (wave trough) in one cycle (Fig. 4.1). The dimensionless quantities η'_{max} and η'_{min} are defined as

$$\eta'_{max} = \eta_{max} / h; \qquad \eta'_{min} = \eta_{min} / h, \tag{4.1}$$

where h is liquid depth.

Dimensionless Amplitude Base Shear Force. Under a sinusoidal excitation, the base shear force $F(t)$ has the same amplitude F_m either in positive direction or negative direction (Fig. 4.1). F_m is nondimensionalized by the maximum inertia force of liquid treated as a solid mass in sinusoidal motion:

$$F'_m = F_m / (m_w \omega^2 A), \tag{4.2}$$

where $\omega = 2\pi f$, is the angular excitation frequency.

Dimensionless Energy Loss per Cycle. The shaking table inputs energy into the TLD, and the TLD itself dissipates energy, ΔE due to liquid sloshing. When TLD is at steady state, it means that in each cycle of excitation, the energy input into the TLD equals the energy dissipation inside the TLD. The energy input into the TLD, E_{input} can be calculated from the base shear force F and the displacement of shaking table x_s, which are both the functions of time. Thus the energy dissipation per cycle, ΔE can be calculated as

$$\Delta E = E_{input} = \int_t^{t+T} F(t)\, dx_s(t), \tag{4.3}$$

where T is the period of excitation, i.e. $2\pi/\omega$. From the above equation, we know that the energy dissipation per cycle depends both on the amplitudes of F and x_s and on the phase difference between them. ΔE is nondimensionalized as follows,

$$\Delta E' = \Delta E / (\frac{1}{2} m_w (\omega A)^2). \tag{4.4}$$

Note that $m_w(\omega A)^2/2$ is just a reference value to nondimensionalize but not the energy of liquid sloshing.

Response Amplitude of Structure attached with TLD. In TLD-sturcture interaction experiment, the response amplitude of structure attached with TLD

was measured. This quantity is employed for present the results of TLD-structure interaction, from which one can see the efficiency of TLD.

4.2 TLD SUBJECTED TO HORIZONTAL MOTION

4.2.1 Time Histories

The wave forms of these time histories vary as the excitation frequency or the base amplitude varies. Unsymmetrical wave form can be observed even under the harmonic excitation of small amplitude (Fig. 4.1b). At certain excitation frequencies, two or three waves can be observed in one cycle (e.g., Fig. 4.1c).

Figure 4.2 presents the measured transient time history responses of liquid surface elevation, η_0 and that of base shear force, F, for the input base amplitude $A = 0.25\ cm$. The wave forms of liquid motion vary as the excitation frequency changes. At $f/f_w = 1.001$, two waves in one cycle can be observed. This is a nonlinear effect of the second higher-harmonic of liquid sloshing, which is excited at an excitation frequency about one third of the natural frequency of second unsymmetrical mode of liquid sloshing. At $f/f_w = 0.951$, even the third higher-harmonic can be observed clearly. For shallow liquid sloshing in a rectangular tank, the natural frequencies are related as $\omega_2 \approx 3\omega_1$, $\omega_3 \approx 5\omega_1$ (ω_n: the natural frequencies of n^{th} higher-harmonics) (Eq.(2.25)). Near the fundamental resonance, quadratic nonlinearity and cubic nonlinearity induce coupling with the 2nd and the 3rd higher-harmonics, respectively, thereby changing the liquid sloshing qualitatively (Nayfeh and Mook 1979).

Numerical simulations corresponding to these cases are also shown for comparison. In numerical simulation, the liquid motion of TLD was assumed to be quiescent at $t=0$. The time increment was $1/60$ of the excitation period of shaking table. The computation was carried on until 80 periods where liquid sloshing was regarded to have reached steady state. Comparing the numerical simulation with the experimental results, good agreement can be seen. The TLD model developed here is satisfactory in predicting not only the fundamental resonance but also the nonlinearity which induces the effects of higher-harmonics of liquid sloshing.

Figure 4.3 shows some examples of force-displacement diagrams for the base displacement amplitude of $0.25\ cm$. One can find also in Fig. 4.3 that the simulation results agree well with those of the experiment.

Figure 4.2 The time histories of base shear force, F (Base amplitude A=0.25 cm).

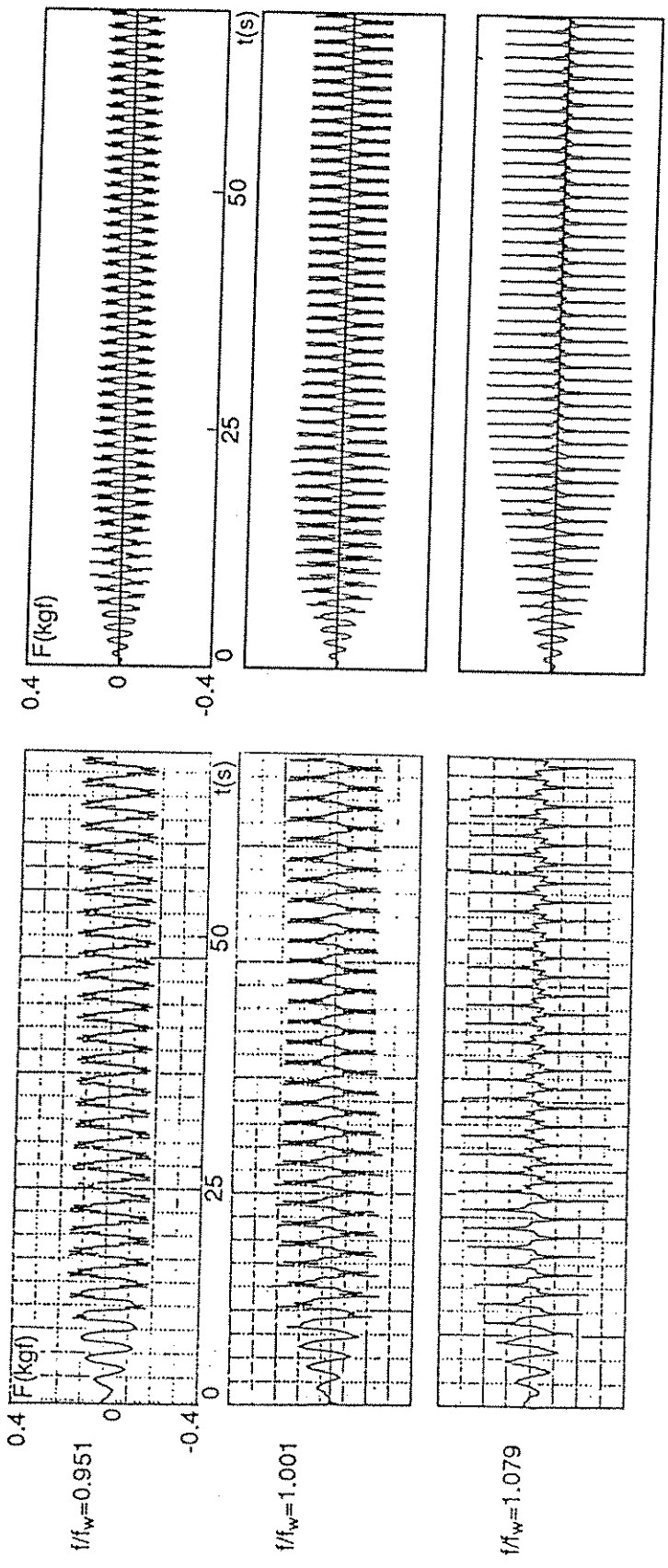

Figure 4.3 The energy dissipation loops (Base amplitude A=0.25 cm).

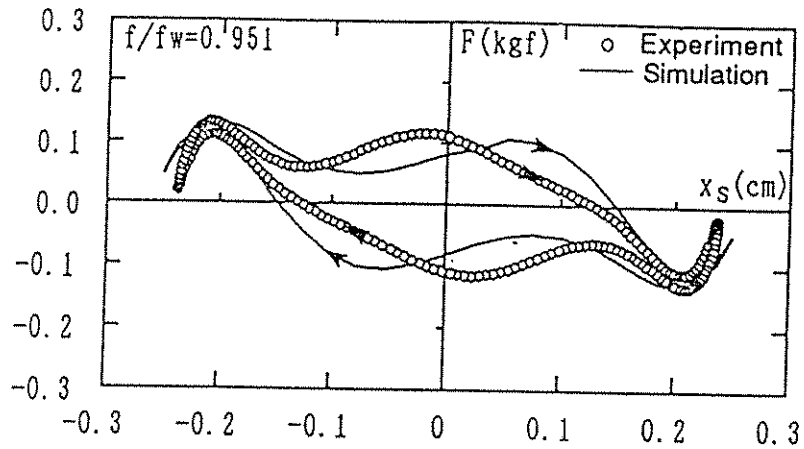

(a) f/f_w=0.951

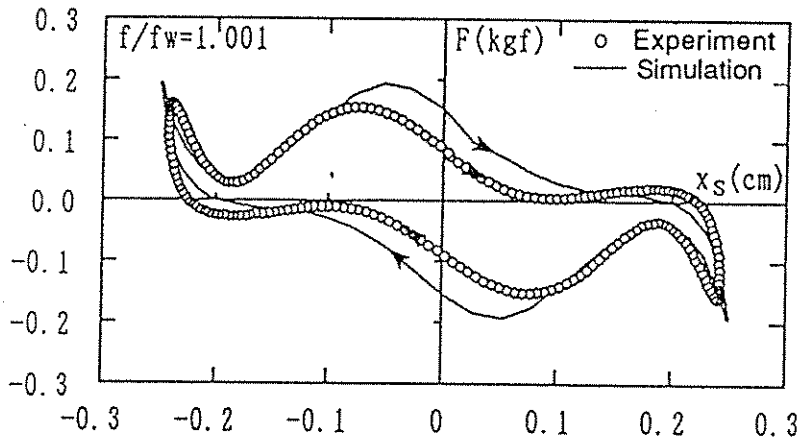

(b) f/f_w=1.001

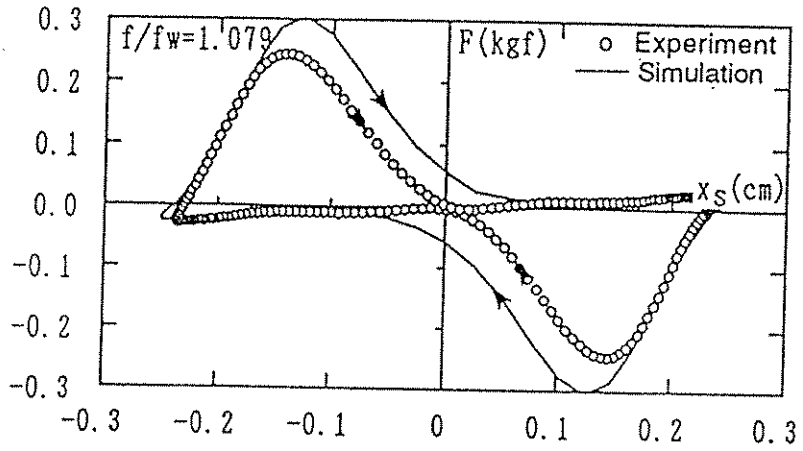

(c) f/f_w=1.079

Figure 4.4 Frequency responses of η'_{max} and η'_{min}, F'_m, and $\Delta E'$.

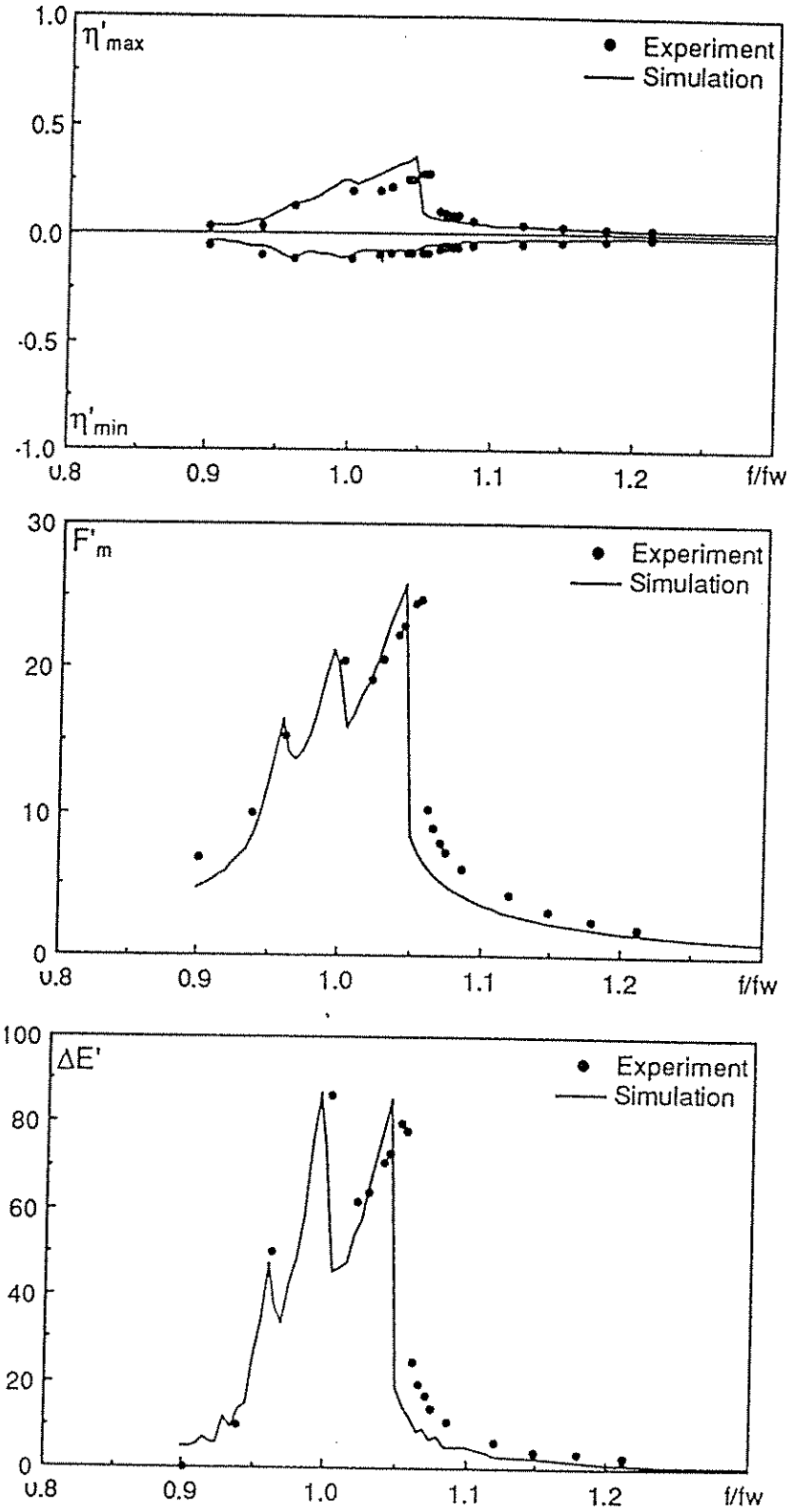

(a) Base Amplitude = 0.1 cm

Figure 4.4 (Continued).

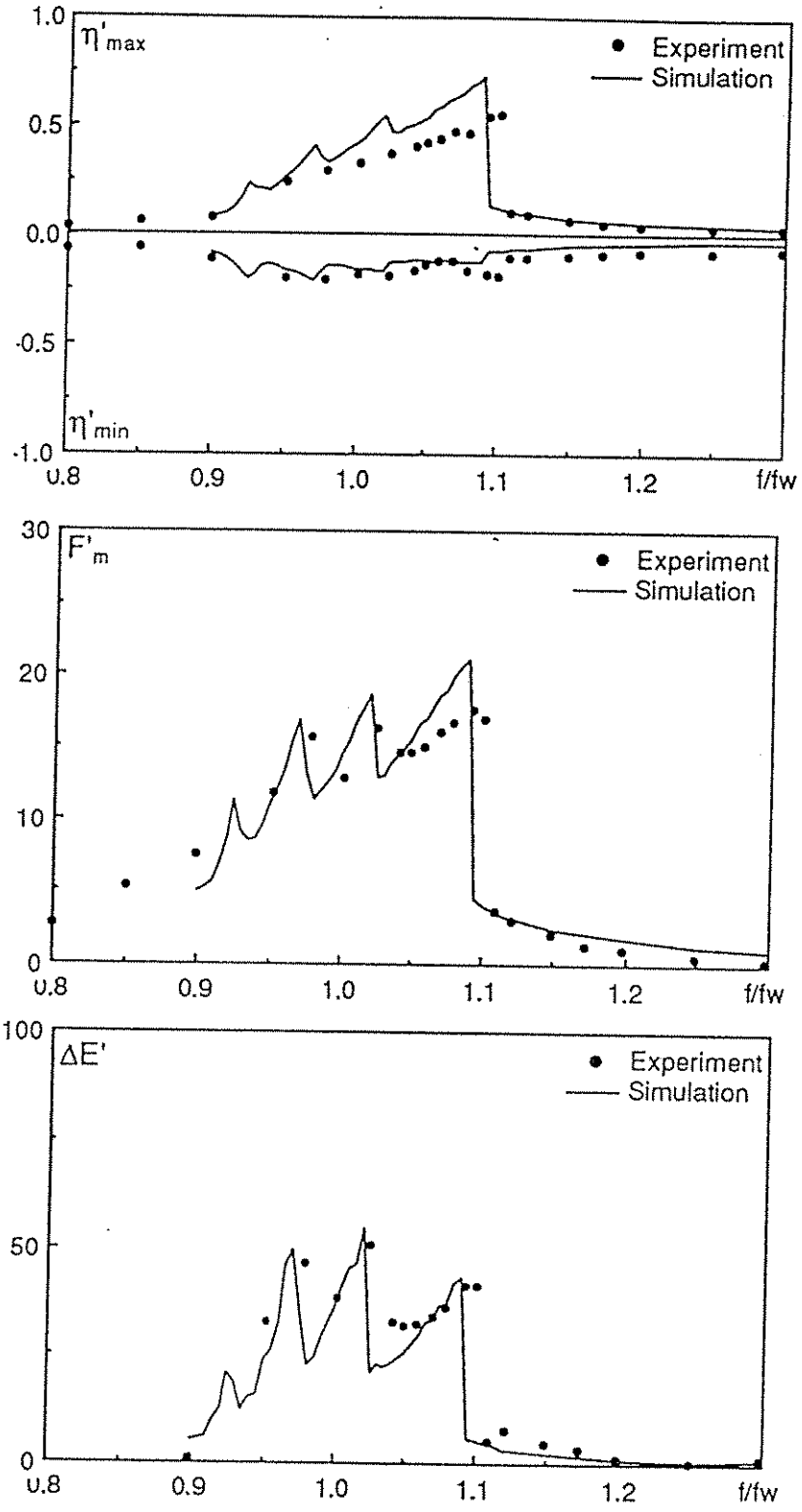

(b) Base Amplitude = 0.25 cm

Figure 4.4 (Continued).

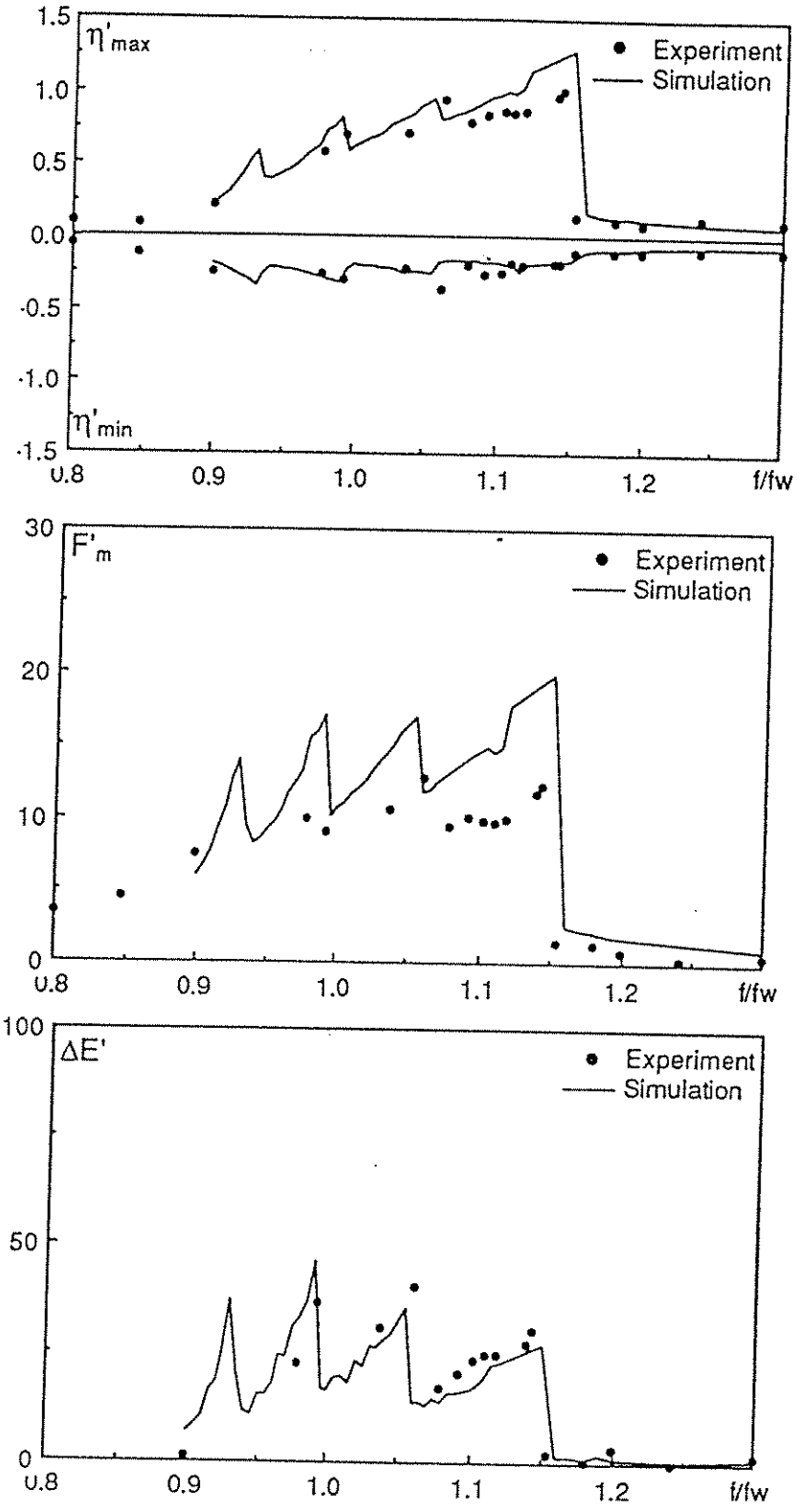

(c) Base Amplitude = 0.5 cm

Figure 4.4 (Continued).

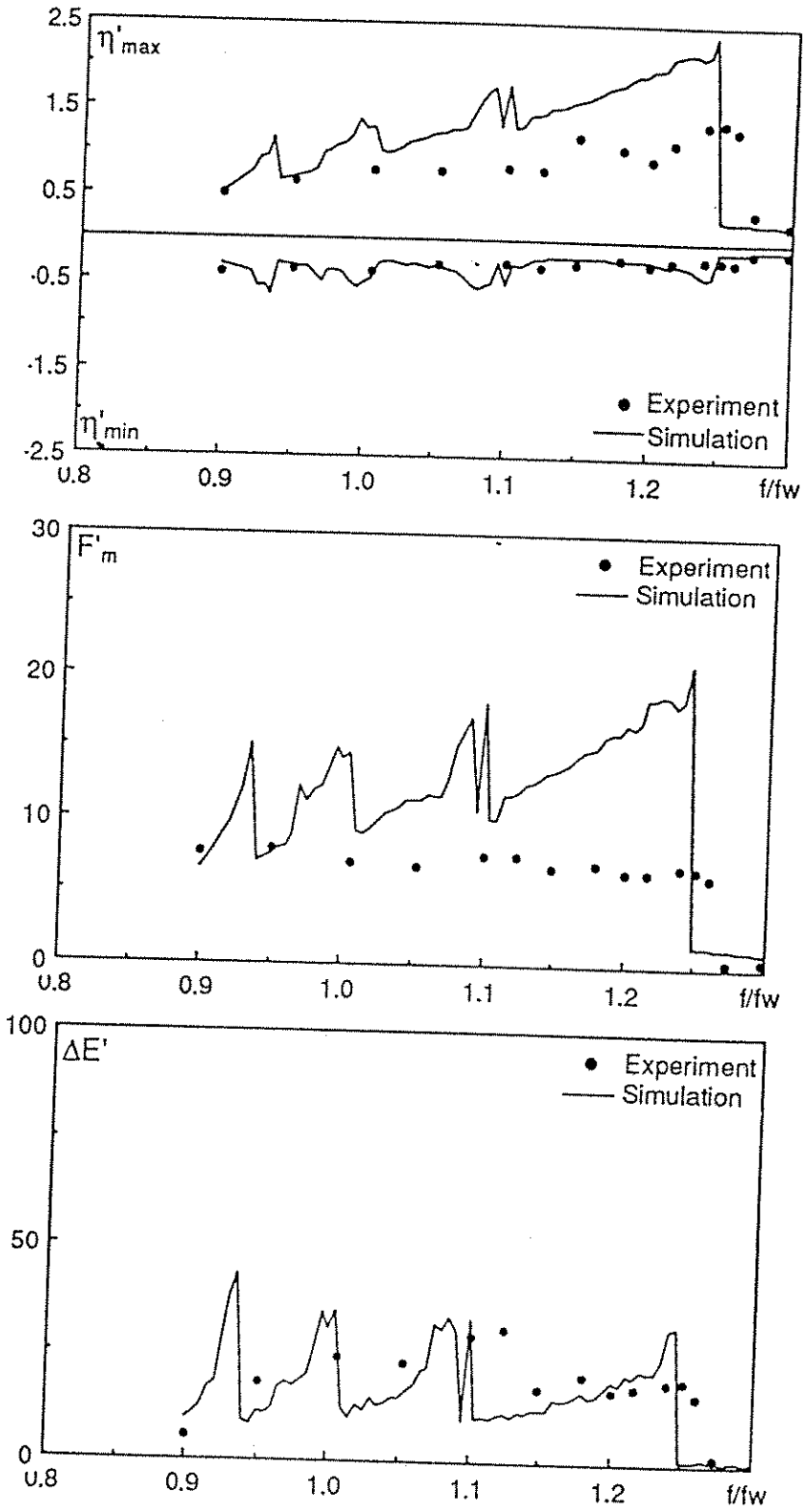

(d) Base Amplitude = 1.0 cm

4.2.1 Frequency Responses

In Fig.4.4, the nondimensionalized quantities, η'_{max} , η'_{min} (surface elevation), F'_m (maximum base shear force) and $\Delta E'$ (energy loss in TLD per cycle) are plotted for the frequency ratio range of $0.9 < f/f_w < 1.3$.

All of the cases in the experiment indicate that the liquid motions possess strong nonlinearity (Fig. 4.4a to d). The fundamental resonant frequency ratio is greater than *1.00* even for the smallest input amplitude case *(A = 0.1 cm)*. At a certain value of frequency ratio larger than *1.00*, η'_{max} and η'_{min} jumps, indicating that the nonlinearity of liquid sloshing is a "hardening spring" type. As the input amplitude increases, the resonant frequency becomes larger. The resonant frequency for the base amplitude of *0.1 cm* is about $1.1f_w$ and increases to about $1.25f_w$ for the base amplitude of *1.0 cm*. This indicates that the nonlinearity becomes stronger.

Local peaks of η'_{max} (and also of F'_m and $\Delta E'$) at the frequency range less than the fundamental resonant frequency, can be observed in Fig.4.4a, b and c. These are due to the appearance of higher harmonics as seen in Figs. 4.1 and 4.2.

For the relatively small amplitude excitation *(0.1 cm, 0.25 cm, 0.5 cm)*, the simulation can predict the experimental results well. For the input amplitude of *1.0 cm*, however, the wave height exceeded the liquid depth, *h* and the existences of breaking waves were also visually identified (Fig. 4.4d). In this case, the simulation results do not agree with those of the experiments. The simulation overestimates η'_{max} and F'_m, although the resonant frequency ratio is well predicted. It should be noticed in Fig. 4.4d that the simulation underestimates $\Delta E'$ in the range $1 < f/f_w < 1.25$. This is probably because the energy dissipation for the base displacement amplitude of *1.0 cm* or larger is due not only to viscosity of liquid but also to breaking waves. All these results indicate that the TLD model developed here is valid as far as the continuous free surface condition is satisfied. In further increases of the base amplitude, *A (>1.0 cm)*, η'_{max} , η'_{max} , F'_m and $\Delta E'$ did not show clear resonance peaks and became very flat over a wide range of f/f_w (Sun, et al. 1989).

In practice, the vibration amplitudes of structure may be in a range where breaking waves in TLD occur. To make the TLD model valid even in wave breaking condition, the model is modified. The modified model is found to be able to explain the experimental results well [Sun et al. 1990]. The details are given in Sections 2.4 and 5.4.

4.3 TLD SUBJECTED TO PITCHING MOTION

4.3.1 Time Histories

As a sample, the time histories of wave surface elevation near the end wall of the TLD tank are shown in Fig. 4.5 for the case R6N1-01 (Table 3.6) ($h=3.0cm$, $\theta_0=0.1\ deg$). The wave motion is almost linear at the range of low frequency ($f/f_w=0.85$), and than becomes unsymmetrical about the still water level surface as the increasing of the wave amplitude. The higher harmonic waves, i.e., more than 2 peaks in one cycle of excitation can be observed. At $f/f_w=1.10$, the wave amplitude jumps down, and then the wave sloshing becomes linear. The other cases in Table 3.6 also demonstrate the same trend. These phenomena are similar to those in the experiment of TLD subjected to horizontal motion, and indicate that the nonlinearities of shallow liquid sloshing is strong.

4.3.2 Frequency Response

The experiment results of the frequency response of η'_{max} and η'_{min} as defined in Section 4.1 are shown in Fig. 4.6. The numerical simulations were also carried out corresponding to the experimental cases. In the computation, the TLD was excited from rest, and the computation continued until 120 periods of excitation, where the response of liquid motion was regarded to be steady state. The values of η'_{max} and η'_{min} are calculated by taking average value in last 20 cycles. The excitation frequency swept within the range of $0.8 \le f/f_s \le 1.2$ with a interval of 0.005.

From Fig. 4.6, it is found again that the nonlinearities of liquid sloshing are similar to those in TLD subjected to horizontal motion. The results of the case R6N1-01 (Fig. 4.6a) shows a good agreement between the experiment and simulation. However, for the cases R6N1-02 (Fig. 4.6b) and R6N1-03 (Fig. 4.6c), the simulation values are larger than the experimental ones. This may be due to the underestimated damping of liquid sloshing in the simulation. For the case of R6N1-04, the agreement around the resonance was not so satisfactory. This disagreement may due to that the experimental equipment could not generate purely sinusoidal motion as described in the sub-section 3.2.1. Several examples of time histories of the base displacement θ for the case R6N2-01 are shown in Fig. 4.7. It can be observed that the motion are not sinusoidal.